DYNAMIC PROBLEMS OF RATE-AND-STATE FRICTION IN VISCOELASTICITY

ELIAS PIPPING

Inauguraldissertation zur Erlangung der Doktorwürde

Mathematisches Institut
Fachbereich Mathematik und Informatik
Freie Universität Berlin

September 2014

Elias Pipping: *Dynamic problems of rate-and-state friction in viscoelasticity,* © September 2014

BETREUER:
Prof. Dr. Ralf Kornhuber

GUTACHTER:
Prof. Dr. Ralf Kornhuber
Prof. Dr. Onno Oncken
Prof. Dr. Alexander Mielke

TAG DER DISPUTATION:
10. Dezember 2014

PREAMBLE

In this work, the model of rate-and-state friction, which can be viewed as central to the numerical simulation of earthquakes, is considered from a mathematical point of view.

First, a framework is presented through which a general class of such friction laws can be understood and analysed. A prototypical viscoelastic problem of earthquake rupture is then formulated, both in strong and in variational form.
Analysis of this problem is difficult, since the incorporation of rate-and-state friction leads to a coupling of variables. In a time-discrete setting, nonetheless, results on existence, uniqueness, and continuous parameter dependence of solutions can be obtained.
The principal idea is to reformulate the variable interdependence as a fixed point problem and to prove convergence for a corresponding iteration. With that in mind, next, a numerical algorithm is proposed that resolves the coupling through a fixed point iteration. Since it puts a state-of-the-art solver and adaptive time stepping to use, it is not only stable but also fast.
Its applicability to problems of interest is demonstrated in the penultimate chapter, which focuses on simulations of megathrust earthquakes that form at the base of a subduction zone.

The main assumptions made throughout this work are summarised and discussed in the last chapter.

ACKNOWLEDGEMENTS

Funding was generously provided by the Free University of Berlin, which supported me in my first year of research through its Center for Scientific Simulation, and the Helmholtz graduate research school GeoSim, which granted me an additional 3-year scholarship.

PUBLICATIONS

Some ideas and figures have appeared previously in [13].

CONTENTS

1 FRICTION: AN INTRODUCTION

Friction is a macroscopic description of microscopic forces that resist relative motion of touching surfaces. For lack of a better understanding, in physics, friction is usually assumed to obey a few conditions of empirical nature. Two of the main ingredients, known as Amontons' laws, can be stated as follows: The force of friction is

- independent of the apparent area of contact and
- directly proportional to the applied load.

The first assumption tells us that friction can be viewed as a local process that acts at every point on the contact surface. We can thus quantify its effect at any such point by means of a scalar $|\boldsymbol{\sigma}_t|$.[1] In addition, this quantity is proportional to the normal stress $|\sigma_n|$ by the second assumption, so that we have

$$|\boldsymbol{\sigma}_t| = \mu|\sigma_n| \tag{1}$$

with an unknown scalar μ, referred to as the *coefficient of friction*.[2] Any scalar friction model built atop Amontons' laws, therefore, need only provide a way to compute μ.

1.1 RATE-AND-STATE FRICTION

Rate-and-state friction assumes that μ is a function of the sliding velocity or *slip rate* V and a memory or *state* variable α, which is to say

$$\mu = \mu(V, \alpha).$$

This condition is complemented by an evolution equation of the form

$$\dot{\alpha} = \dot{\alpha}(V, \alpha).$$

The state variable α should be thought of here not as a physical quantity but rather as an automaton, which continually consumes velocity information and produces new information, based on a digest of past velocities. The dependence of μ on α is thus another, indirect form of velocity dependence.

1 The expressions $\boldsymbol{\sigma}_t$ and σ_n are properly introduced in the next chapter.

2 In Coulomb's friction law, the normal load dependence is taken to apply to the friction bound rather than the actual force, hence one obtains $|\boldsymbol{\sigma}_t| \leq \mu|\sigma_n|$ in this case.

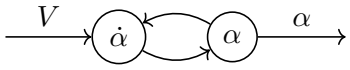

Figure 1.1: The state variable as an automaton.

1.2 THE LAWS OF DIETERICH AND RUINA

For a side-by-side comparison of a few popular laws and the historical background, see [11].

The two oldest yet most commonly used rate-and-state friction laws can be stated as follows.[3]

The *ageing law* (also known as *slowness law*)

$$\mu = \mu_* + a \log \frac{V}{V_*} + b\alpha, \qquad \dot{\alpha} = \frac{V_* e^{-\alpha} - V}{L} \tag{2}$$

and the *slip law*

$$\mu = \mu_* + a \log \frac{V}{V_*} + b\alpha, \qquad \dot{\alpha} = -\frac{V}{L}(\log \frac{V}{V_*} + \alpha). \tag{3}$$

When presented in this form, both laws use the same expression for μ, so that their respective state variables α can be identified. This is also why their names are often used to refer to the state evolution equations only.

1.2.1 *Interpretation*

Both laws contain three non-dimensional parameters a, b, and μ_* as well as a velocity V_* and a length L. The role of these parameters is best explained by means of an experiment with a single degree of freedom, illustrated in figure 1.2: We prescribe the velocity V, let α evolve in accordance with either (2) or (3) — our observations will apply to both laws — and pay special attention to the trajectory of μ.
To that end, let V be constant at $V_1 > 0$ and assume the system to be in steady state, *i.e.* $\alpha = \alpha_{\mathrm{ss}}(V_1) \coloneqq \log(V_*/V_1)$, which means

$$\mu = \mu_{\mathrm{ss}}(V_1) \coloneqq \mu_* + (a - b) \log(V_1/V_*).$$

Now force an instantaneous acceleration to $V_2 > V_1$ and keep the new velocity fixed. This triggers a direct increase in μ of magnitude $a \log(V_2/V_1)$. In addition, over time, the state α evolves towards $\alpha_{\mathrm{ss}}(V_2)$, which leads to a decrease in μ of magnitude $b \log(V_2/V_1)$. The parameters a and b thus act as weights for both effects. The overall change of μ is given by

$$\mu_{\mathrm{ss}}(V_2) - \mu_{\mathrm{ss}}(V_1) = (a - b) \log(V_2/V_1).$$

3 In the literature, these laws are usually stated in terms of the state variable $\theta = e^{\alpha} L/V_*$.

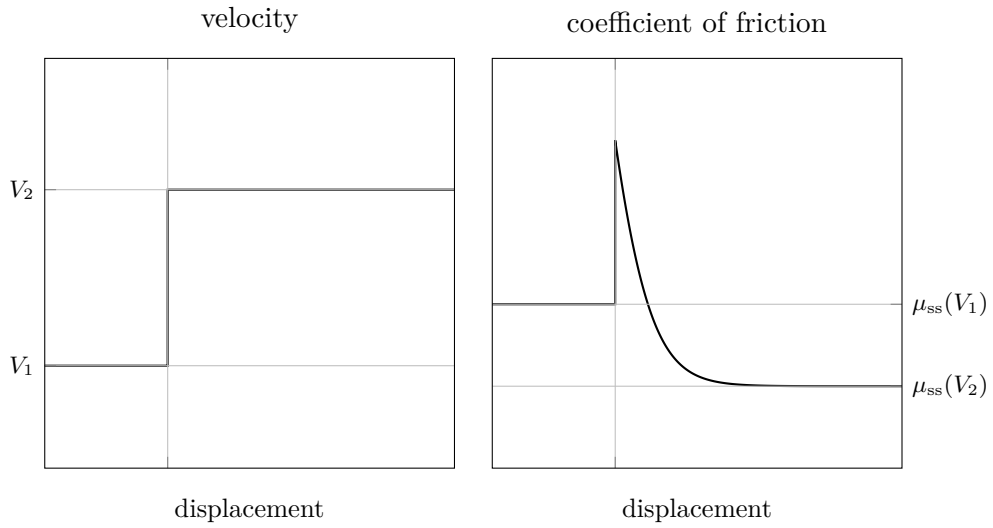

Figure 1.2: Response of the friction coefficient to a jump in velocity. Simulation with the ageing law.

Whether this quantity is positive or negative depends on the sign of the constant $a - b$, see also remark 1.1.
A look at the state evolution laws reveals that L/V acts as a time scale: the smaller the length L, the more quickly the state evolves; the length L thus bears traits of a regularisation parameter. The parameter μ_*, finally, is the steady state coefficient of friction corresponding to the arbitrarily chosen velocity V_* and defined through the relation $\mu_{ss}(V_*) = \mu_*$.

Remark 1.1 (Rate-weakening and -strengthening)**.** *In the context of friction, material can be called* rate-weakening *or* rate-strengthening*. In the former case, an increase in sliding velocity weakens it further, leading to a smaller friction coefficient and thus an even greater sliding velocity; in the latter case, it shows the opposite behaviour.*
In a simple law of the form

$$\mu = \mu(V),$$

the velocity dependence of μ would have to be negative, were it to model rate-weakening — a property which is known to lead to mathematical issues and physical absurdities, see [14].
Through its two types of velocity dependence, rate-and-state friction circumvents this issue: The direct effect is required to be monotone but the state effect is not. As a result, the immediate response to velocity increases is always positive, yet the overall response after a finite amount of time can very well be negative.

1.2.2 *Issues*

In their original, above-stated form, the laws of Dieterich and Ruina employ the term $\log(V/V_*)$, which becomes arbitrarily negative for velocities V close to zero; consequently, we have

$$\mu(V,\alpha) \to -\infty \qquad \text{whenever } V \to 0$$

for fixed α. These laws are thus unphysical for sufficiently small V, since they predict a negative coefficient of friction; for $V = 0$, moreover, they are not even mathematically sound. If we introduce the *sign-change velocity*

$$V_\alpha = V_* \exp\biggl(-\frac{\mu_* + b\alpha}{a}\biggr),$$

this issue becomes even clearer, since now μ can be written as

$$\mu(V,\alpha) = a \log \frac{V}{V_\alpha}, \tag{4}$$

so that V_α denotes the velocity at which the coefficient of friction vanishes. In the literature, this shortcoming of the Dieterich–Ruina laws has been addressed by means of regularisation, see [14]. To be precise, the logarithm on the right-hand side of (4) is replaced by the nonnegative function $z \mapsto \operatorname{asinh}(z/2)$, yielding the *regularised law*

$$\mu_\mathrm{r}(V,\alpha) = a \operatorname{asinh}\biggl(\frac{V}{2V_\alpha}\biggr). \tag{5}$$

A different approach, which has been pursued in [13] is to trust the original law as much as possible, and only modify it whenever it predicts a negative coefficient of friction. The requirement of monotonicity then leads to the *truncated law*

$$\mu_\mathrm{t}(V,\alpha) = a \log^+ \frac{V}{V_\alpha} \qquad \text{with} \qquad \log^+ z = \begin{cases} \log z & \text{if } z \geq 1 \\ 0 & \text{otherwise.} \end{cases} \tag{6}$$

Both formulations differ so little, however, that the distinction is irrelevant in practice.

It should be noted that rate-and-state friction laws generally do not specify how V should be interpreted — or more generally, how α should evolve — if two bodies undergoing rate-and-state friction suddenly lose contact. This issue originates in the lack of a consistent physical interpretation of the state variable α.

1.3 A GENERAL FRAMEWORK

In this section, a general formulation of rate-and-state friction is proposed which covers the Dieterich–Ruina laws as special cases.

More technical assumptions will be required and introduced in later sections.

A rate-and-state friction law shall be given by two functions

$$\mu\colon (V,\alpha) \mapsto \mu(V,\alpha),$$
$$\dot{\alpha}\colon (V,\alpha) \mapsto \dot{\alpha}(V,\alpha)$$

defined for nonnegative V and arbitrary α, which meet the following criteria.

(A1) The function μ is not only nonnegative but also nondecreasing in its first argument and satisfies $\mu(0, \cdot\,) = 0$.

(A2) The function μ is uniformly Lipschitz in its second argument. In other words, we have

$$|\mu(V,\alpha) - \mu(V,\beta)| \le L_\mu |\alpha - \beta|$$

for any α, β, and V.

(A3) The function $\dot{\alpha}$ is nonincreasing and continuous in its second argument.

As intended, this framework contains the examples from the previous section.

Proposition 1.2. *Consider the ageing law (2) or the slip law (3), either regularised as per (5) or truncated as per (6). Then each of the four resulting laws satisfies assumptions (A1) to (A3).*

Proof. That μ_r and μ_t satisfy the assumptions (A1) and (A3) is obvious. To show that μ_r satisfies assumption (A2), it suffices to prove

$$|\mu_\mathrm{r}(V,\alpha) - \mu_\mathrm{r}(V,\beta)| = \left|\operatorname{asinh}\left(\frac{V}{2V_\alpha}\right) - \operatorname{asinh}\left(\frac{V}{2V_\beta}\right)\right| \le \left|\log\frac{V_\beta}{V_\alpha}\right|$$

for any α, β, and $V \ge 0$, since the right-hand side equals $b/a \cdot |\alpha - \beta|$. For $V = 0$, this is immediate; for $V > 0$, it becomes clear once we prove the more general claim

$$|\operatorname{asinh}(x) - \operatorname{asinh}(y)| \le |\log x - \log y|$$

for x, $y > 0$. Without loss of generality, assume $x \ge y$, so that we need to show

$$\operatorname{asinh}(x) - \operatorname{asinh}(y) \le \log x - \log y.$$

From the logarithmic representation of the asinh function, we obtain that this is equivalent to

$$\log\frac{x + \sqrt{x^2+1}}{y + \sqrt{y^2+1}} \le \log\frac{x}{y}$$

and thus

$$y\sqrt{x^2+1} \le x\sqrt{y^2+1}$$

which is obviously true. For μ_{t}, we proceed analogously and prove

$$|\mu_{\mathrm{t}}(V,\alpha) - \mu_{\mathrm{t}}(V,\beta)| = \left|\log^+ \frac{V}{V_\alpha} - \log^+ \frac{V}{V_\beta}\right| \leq \left|\log \frac{V_\beta}{V_\alpha}\right|.$$

Again, this is trivially true if $V = 0$. For $V > 0$, we have

$$\begin{aligned}\left|\log^+ \frac{V}{V_\alpha} - \log^+ \frac{V}{V_\beta}\right| &= \left|\max\left\{\log \frac{V}{V_\alpha}, 0\right\} - \max\left\{\log \frac{V}{V_\beta}, 0\right\}\right| \\ &\leq \left|\log\left(\frac{V}{V_\alpha}\right) - \log\left(\frac{V}{V_\beta}\right)\right|\end{aligned}$$

and thus the claim. □

2 CONTINUUM MECHANICS

This introduction to continuum mechanics follows [9] rather closely.

Consider a block that slides along the surface of a rigid foundation, over a time interval $[0, T]$. The block at time zero can then be assumed to be representable through a bounded Lipschitz domain $\Omega \subset \mathbb{R}^d$.
At any later time t, points originally located at a position $\boldsymbol{x} \in \Omega$ will occupy a typically different position $\boldsymbol{y}(t, \boldsymbol{x})$, giving rise to the *motion* $\boldsymbol{y}$.
To describe the change in shape that the block undergoes, we need to differentiate this field of motion in space. Through $\boldsymbol{y}$, we have access to two different coordinate systems: one relative to the *reference configuration* and one relative to the *current configuration*, which undergoes the same motion as Ω. Depending on the situation, it could be more convenient to work with one or the other and in a general setting, it would make a difference with respect to which of the two derivatives are taken.
Not in this work, however. As is often done, we make the assumption of *infinitesimal deformation*; a change of variables between the two coordinate systems must now involve a Jacobian of approximately unity, making them close to indiscernible. To be precise, we write $\boldsymbol{u}$ for the *displacement*, *i.e.* $\boldsymbol{u}(\boldsymbol{x}) = \boldsymbol{y}(\boldsymbol{x}) - \boldsymbol{x}$ for any $\boldsymbol{x} \in \Omega$, and assume the *displacement gradient* $\nabla \boldsymbol{u}$ to be infinitesimally small in comparison to unity.
In this setting, higher-order terms in $\nabla \boldsymbol{u}$ are naturally neglected, too, which means that we can identify the nonlinear *strain tensor* given by

$$\frac{1}{2}\Big(\nabla \boldsymbol{u} + (\nabla \boldsymbol{u})^T + (\nabla \boldsymbol{u})^T \nabla \boldsymbol{u}\Big)$$

in terms of $\boldsymbol{u}$, with the *linearised strain tensor* $\boldsymbol{\varepsilon}$, which satisfies

$$\boldsymbol{\varepsilon}(\boldsymbol{u}) = \frac{1}{2}\Big(\nabla \boldsymbol{u} + (\nabla \boldsymbol{u})^T\Big),$$

an assumption that by itself is referred to as *infinitesimal strain*.

2.1 STRESS AND STRAIN

The strain tensor plays an important role in elasticity. It allows us to split any motion into two components: a *rigid motion* consisting of rotation and translation, which does not produce strain, and another component, which does. Intuitively then, it is clear that strain should correspond to stress, and as a matter of fact, the assumption of elasticity allows us to convert strains into stresses and vice versa seamlessly; but what is stress exactly?

Let $\boldsymbol{x}$ be an interior point of Ω. Now cut Ω in two by means of a smooth surface containing $\boldsymbol{x}$. Along this surface, where the two halves of Ω are in contact, each half exerts a force on the other; normalised with respect to the the area of the surface this gives rise to the stress field $\boldsymbol{s}$ and thus in particular a *stress vector* $\boldsymbol{s}(\boldsymbol{x})$ at $\boldsymbol{x}$. By Newton's third law, the stress must change sign when we change perspective from one half to the other. Even more is true, though: The *Euler-Cauchy stress principle* asserts that $\boldsymbol{s}(\boldsymbol{x})$ depends only on the choice of the separating surface (and thus the two halves of Ω) through its *outer unit normal* $\boldsymbol{n}(\boldsymbol{x})$ at $\boldsymbol{x}$, and that it does so in a linear fashion; in other words, there is a tensor $\boldsymbol{\sigma}(\boldsymbol{x})$ that satisfies $\boldsymbol{s} = \boldsymbol{\sigma}\boldsymbol{n}$. This tensor is referred to as the *stress tensor*.
With all the necessary notation available, now, Hooke's law of linear elasticity can be stated as

$$\boldsymbol{\sigma} = \boldsymbol{\mathcal{B}}\boldsymbol{\varepsilon},$$

where $\boldsymbol{\mathcal{B}}$ is the elasticity tensor of the material in question. The Kelvin–Voigt model for viscoelasticity, similarly, takes the simple form

$$\boldsymbol{\sigma} = \boldsymbol{\mathcal{A}}\dot{\boldsymbol{\varepsilon}} + \boldsymbol{\mathcal{B}}\boldsymbol{\varepsilon}$$

with an additional viscosity tensor $\boldsymbol{\mathcal{A}}$.

2.2 FRICTION

An extension of the stress tensor $\boldsymbol{\sigma}$ to the closure of the domain Ω allows us to obtain the *surface traction* $\boldsymbol{t}$ on $\partial\Omega$ from the outer unit normal[1] $\boldsymbol{n}$ via $\boldsymbol{t} = \boldsymbol{\sigma}\boldsymbol{n}$.
Now fix a point $\boldsymbol{x}$ on the boundary $\partial\Omega$ where the body is in contact with the foundation and decompose the traction $\boldsymbol{t}(\boldsymbol{x})$ into a scalar normal component (the *normal stress*) $\sigma_n = \boldsymbol{t}\cdot\boldsymbol{n}$ as well as a vectorial tangential component (the *shear stress*) $\boldsymbol{\sigma}_t = \boldsymbol{t} - \sigma_n\boldsymbol{n}$. This allows us to postulate the scalar friction law

$$|\boldsymbol{\sigma}_t| = \mu|\sigma_n| + C,$$

which is slightly more general than (1) since it contains a constant $C \geq 0$ representing *cohesion*.
In this manner, we can constrain the magnitude of $\boldsymbol{\sigma}_t$, but we also need to prescribe its direction: First, we require bilateral contact between body and foundation, which is to say $\dot{\boldsymbol{u}} \cdot \boldsymbol{n} = 0$, allowing $\boldsymbol{x}$ to move tangentially only. As the second step, then, in analogy with Coulomb's friction law, we assume that frictional forces resist motion directly, so that

$$-|\dot{\boldsymbol{u}}|\boldsymbol{\sigma}_t = |\boldsymbol{\sigma}_t|\dot{\boldsymbol{u}}.$$

1 Since we assume Ω to be a Lipschitz domain, the outer normals exist almost everywhere on $\partial\Omega$.

The model of rate-and-state friction from section 1.3 can now be understood as

$$\begin{aligned} -\boldsymbol{\sigma}_t &= \frac{\mu(|\dot{\boldsymbol{u}}|, \alpha)|\sigma_n| + C}{|\dot{\boldsymbol{u}}|}\dot{\boldsymbol{u}} && \text{for } \dot{\boldsymbol{u}} \neq 0 \text{ and} \\ |\boldsymbol{\sigma}_t| &\leq C && \text{for } \dot{\boldsymbol{u}} = 0. \end{aligned}$$

Remark 2.1. *The normal stress σ_n generally depends on the displacement $\boldsymbol{u}$ — a source of great mathematical difficulties in the treatment of friction. Since the rate-and-state laws under consideration here have been derived in the setting of constant normal stress, however, and cannot be applied to different regimes, we need to assume a constant normal stress here as well. Once it is constant, it is known.*
To simplify the analysis and notation some more, both the normal stress and any parameters that μ might contain are taken to be uniform in space, too. A discussion of the consequences can be found in the chapter 6.

2.3 CONSERVATION LAWS

According to Newton's laws of motion, in a closed system, at least two (vectorial) quantities should be conserved: Linear momentum and angular momentum.
If the system is not closed, linear momentum does not remain constant but changes at a rate equal to the sum of external forces. If we write ρ for the density field of Ω, and assume it to be constant in time, then the change of linear momentum $\rho\dot{\boldsymbol{u}}$ over time equals $\rho\ddot{\boldsymbol{u}}$. By the above, this vector must balance with the surface forces (or equivalently, by the divergence theorem, the internal flux) and the body force $\boldsymbol{b}$. We thus obtain the central equation

$$\nabla \cdot \boldsymbol{\sigma} + \boldsymbol{b} = \rho\ddot{\boldsymbol{u}}.$$

Balance of angular momentum, additionally, implies that the tensor $\boldsymbol{\sigma}$ is symmetric.

2.4 THE STRONG PROBLEM

Viscoelastic problems with bilateral contact and friction (in subdifferential form) are discussed in Section 13.4 of [9].

We can now combine the insights from the previous sections to obtain a system of equations that govern the motion of a sliding block. Consider again a viscoelastic body (represented by the bounded Lipschitz domain Ω) in bilateral contact with a rigid foundation and subject to rate-and-state friction in the sense of section 1.3.
I will assume the boundary $\Gamma := \partial\Omega$ to consist of three disjoint parts, namely the Neumann boundary Γ_N, the Dirichlet boundary Γ_D, and the

contact boundary Γ_C, on which friction occurs. A typical such situation is depicted in figure 2.1.

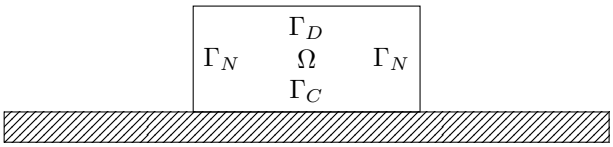

Figure 2.1: The prototypical sliding block.

If the state field α on Γ_C were known throughout the whole time interval of interest $I := [0, T]$, then determining the motion that Ω undergoes would be tantamount to solving the following problem.

Problem 2.1. Find a displacement field $\boldsymbol{u} \in C^2(I, C^2(\bar{\Omega}))$ satisfying

$$\boldsymbol{\sigma} = \boldsymbol{\mathcal{A}}\boldsymbol{\varepsilon}(\dot{\boldsymbol{u}}) + \boldsymbol{\mathcal{B}}\boldsymbol{\varepsilon}(\boldsymbol{u}) \qquad \text{in } \Omega \times I \tag{7}$$

$$\nabla \cdot \boldsymbol{\sigma} + \boldsymbol{b} = \rho \ddot{\boldsymbol{u}} \qquad \text{in } \Omega \times I, \tag{8}$$

and subject to the boundary conditions

$$\dot{\boldsymbol{u}} = 0 \qquad \text{on } \Gamma_D \times I \tag{9}$$

$$\boldsymbol{t} = 0 \qquad \text{on } \Gamma_N \times I \tag{10}$$

$$\dot{\boldsymbol{u}} \cdot \boldsymbol{n} = 0 \qquad \text{on } \Gamma_C \times I \tag{11}$$

$$\left.\begin{aligned} -\boldsymbol{\sigma}_t &= \frac{\mu(|\dot{\boldsymbol{u}}|, \alpha)|\sigma_n| + C}{|\dot{\boldsymbol{u}}|}\dot{\boldsymbol{u}} && \text{for } \dot{\boldsymbol{u}} \neq 0 \\ |\boldsymbol{\sigma}_t| &\leq C && \text{for } \dot{\boldsymbol{u}} = 0 \end{aligned}\right\} \qquad \text{on } \Gamma_C \times I \tag{12}$$

as well as initial conditions on $\boldsymbol{u}$ and $\dot{\boldsymbol{u}}$.

In general, however, the state field will not be known. Conversely, if we knew the displacement field $\boldsymbol{u}$ throughout the entire time interval I, we could solve the following family of ordinary differential equations to obtain α.

Problem 2.2. Find a state field $\alpha \in C^1(I, C(\Gamma_C))$ which satisfies

$$\dot{\alpha} = \dot{\alpha}(|\dot{\boldsymbol{u}}|, \alpha) \qquad \text{on } \Gamma_C \times I.$$

as well as an initial condition.

But since we usually know neither $\boldsymbol{u}$ nor α, our task has to be summarised as this:

Problem 2.3. Find a pair $(\boldsymbol{u}, \alpha)$ such that $\boldsymbol{u}$ solves problem 2.1 with respect to the state field α and α solves problem 2.2 with respect to the velocity field $\dot{\boldsymbol{u}}$.

2.5 THE WEAK PROBLEM

For an introduction to variational inequalities, see Chapter 6 of [8].

In what follows, we will derive a *weak formulation* of problem 2.1. Assuming a sufficiently smooth solution, we can test (8) at a fixed point in time with functions $\boldsymbol{v}$ from the space

$$\mathcal{V} = \{\boldsymbol{v} \in H^1(\Omega)^d \colon \boldsymbol{v} = 0 \text{ on } \Gamma_D,\ \boldsymbol{v} \cdot \boldsymbol{n} = 0 \text{ on } \Gamma_C\}$$

and apply integration by parts to find

$$\int_\Omega \rho \ddot{\boldsymbol{u}} \cdot \boldsymbol{v} + \int_\Omega \boldsymbol{\sigma} \colon \nabla \boldsymbol{v} = \int_\Gamma \boldsymbol{t} \cdot \boldsymbol{v} + \int_\Omega \boldsymbol{b} \cdot \boldsymbol{v} \quad \forall \boldsymbol{v} \in \mathcal{V}. \tag{13}$$

Since $\boldsymbol{\sigma}$ is symmetric, the term $\nabla \boldsymbol{v}$ in (13) can be replaced with its symmetrisation $\boldsymbol{\varepsilon}(\boldsymbol{v})$; using (7) we then obtain

$$\int_\Omega \rho \ddot{\boldsymbol{u}} \cdot \boldsymbol{v} + \int_\Omega \boldsymbol{\mathcal{A}}\boldsymbol{\varepsilon}(\dot{\boldsymbol{u}}) \colon \boldsymbol{\varepsilon}(\boldsymbol{v}) + \int_\Omega \boldsymbol{\mathcal{B}}\boldsymbol{\varepsilon}(\boldsymbol{u}) \colon \boldsymbol{\varepsilon}(\boldsymbol{v}) = \int_\Gamma \boldsymbol{t} \cdot \boldsymbol{v} + \int_\Omega \boldsymbol{b} \cdot \boldsymbol{v}$$

for any $\boldsymbol{v} \in \mathcal{V}$. This variational equation can also be phrased more abstractly once we introduce the right operators and functionals; indeed, with

$$\begin{aligned}
\ell &\colon \mathcal{V} \to \mathbb{R},\ \boldsymbol{v} \mapsto \int_\Omega \boldsymbol{b} \cdot \boldsymbol{v} \\
\mathcal{M} &\colon \mathcal{V}^* \to \mathcal{V}^*,\ \langle \boldsymbol{v}, \cdot \rangle \mapsto \langle \rho \boldsymbol{v}, \cdot \rangle \\
\mathcal{C} &\colon \mathcal{V} \to \mathcal{V}^*,\ \boldsymbol{v} \mapsto \int_\Omega \boldsymbol{\mathcal{A}}\boldsymbol{\varepsilon}(\boldsymbol{v}) \colon \boldsymbol{\varepsilon}(\,\cdot\,) \\
\mathcal{K} &\colon \mathcal{V} \to \mathcal{V}^*,\ \boldsymbol{v} \mapsto \int_\Omega \boldsymbol{\mathcal{B}}\boldsymbol{\varepsilon}(\boldsymbol{v}) \colon \boldsymbol{\varepsilon}(\,\cdot\,)
\end{aligned}$$

it takes the form

$$\mathcal{M}\ddot{\boldsymbol{u}} + \mathcal{C}\dot{\boldsymbol{u}} + \mathcal{K}\boldsymbol{u} = \int_\Gamma (\boldsymbol{t}, \cdot\,) + \ell. \tag{14}$$

The unknown $\boldsymbol{t}$ still occurs here because we have not yet taken any boundary conditions into account: By (10), it vanishes on Γ_N, and on Γ_D our test functions are identically zero by (9). What remains to be done, then, is to put the friction law (12) into a form that can be used in this context.

Subdifferential boundary conditions

If we were given subdifferential inclusions of the form

$$-\boldsymbol{\sigma}_t \in \partial \psi(\,\cdot\,, \boldsymbol{x})(\dot{\boldsymbol{u}}(\boldsymbol{x})) \tag{15}$$

or equivalently

$$\psi(\boldsymbol{v}, \boldsymbol{x}) \geq \psi(\dot{\boldsymbol{u}}(\boldsymbol{x}), \boldsymbol{x}) - \boldsymbol{\sigma}_t(\boldsymbol{v} - \dot{\boldsymbol{u}}(\boldsymbol{x})) \quad \forall \boldsymbol{v} \in \mathbb{R}^d$$

for $\boldsymbol{x} \in \Gamma_C$ with a family of convex functions $\psi(\,\cdot\,, \boldsymbol{x})$, then we could test them simultaneously with traces[2] of functions in $\mathcal{V}$ to get[3]

$$\int_{\Gamma_C} \psi(\boldsymbol{v}, \boldsymbol{x}) \,\mathrm{d}\boldsymbol{x} \geq \int_{\Gamma_C} \psi(\dot{\boldsymbol{u}}, \boldsymbol{x}) \,\mathrm{d}\boldsymbol{x} - \int_{\Gamma_C} \boldsymbol{\sigma}_t \cdot (\boldsymbol{v} - \dot{\boldsymbol{u}}) \quad \forall \boldsymbol{v} \in \mathcal{V}$$

or equivalently

$$-\int_{\Gamma_C} (\boldsymbol{\sigma}_t, \,\cdot\,) \in \partial j(\dot{\boldsymbol{u}}) \quad \text{with} \quad j \colon \mathcal{V} \to \mathbb{R},\ \boldsymbol{v} \mapsto \int_{\Gamma_C} \psi(\boldsymbol{v}, \boldsymbol{x}) \,\mathrm{d}\boldsymbol{x}.$$

This type of boundary condition thus, too, has a weak form that can serve to complete our problem: It would then read

$$\ell \in \mathcal{M}\ddot{\boldsymbol{u}} + \mathcal{C}\dot{\boldsymbol{u}} + \mathcal{K}\boldsymbol{u} + \partial j(\dot{\boldsymbol{u}}).$$

This leaves us with the task of formulating (12) as a subdifferential inclusion, which is not difficult given the parallels to Tresca's thoroughly investigated friction law: As is easily checked, we can choose

$$\psi(\dot{\boldsymbol{u}}, \boldsymbol{x}) = \bar{\mu}(|\dot{\boldsymbol{u}}|, \alpha(\boldsymbol{x}))|\sigma_n| + C|\dot{\boldsymbol{u}}| \tag{16}$$

with

$$\bar{\mu}(V, \alpha) = \int_0^V \mu(r, \alpha) \,\mathrm{d}r$$

in the terminology of (15). That ψ is convex in its first argument is a consequence of assumption (A1); for non-zero velocities, moreover, the equivalence of (12) and (15) follows immediately from the chain rule. For vanishing $\dot{\boldsymbol{u}}$, note that the condition $\mu(0, \,\cdot\,) = 0$ makes any directional derivative of $\bar{\mu}(|\,\cdot\,|, \boldsymbol{x})$ at zero vanish.
In summary, our weak formulation of problem 2.1 reads

Problem 2.4. Find $\boldsymbol{u} \colon I \to \mathcal{V}$ such that almost everywhere in I, we have $\dot{\boldsymbol{u}} \in \mathcal{V}$, $\ddot{\boldsymbol{u}} \in \mathcal{V}^*$, and

$$\ell \in \mathcal{M}\ddot{\boldsymbol{u}} + \mathcal{C}\dot{\boldsymbol{u}} + \mathcal{K}\boldsymbol{u} + \partial j(\,\cdot\,, \alpha)(\dot{\boldsymbol{u}}),$$

with

$$j(\boldsymbol{v}, \alpha) = \int_{\Gamma_C} \bar{\mu}(|\boldsymbol{v}|, \alpha)|\sigma_n| + C|\boldsymbol{v}| \quad \forall \boldsymbol{v} \in \mathcal{V}$$

By incorporating this weak formulation in the coupled problem 2.3, we obtain the weak coupled problem

Problem 2.5. Find a pair $(\boldsymbol{u}, \alpha)$ such that $\boldsymbol{u}$ solves problem 2.4 with respect to the state field α and α solves problem 2.2 with respect to the velocity field $\dot{\boldsymbol{u}}$.

2 Traces are not marked as such here or in the following sections.
3 Integrals over non-integrable quantities are to be understood as positively infinite here.

2.6 DETOUR: EQUIVALENCE OF BOTH PROBLEMS

By construction, any *strong* solution of problem 2.1 is also a *weak* solution of problem 2.4. The converse, however, does not hold, because a solution to problem 2.4 will generally not be sufficiently regular: We do not require Ω to be smooth or convex and the boundary data on Γ_C can be quite unpleasant.
Under potentially rather restrictive circumstances, the solution $\boldsymbol{u}$ and its time derivatives may be smooth nonetheless.[4] If so, we can revert the weakening process: By definition of the subdifferential, for $\boldsymbol{u}$ to solve problem 2.4 is to satisfy

$$\int_\Omega \rho\ddot{\boldsymbol{u}}\cdot(\boldsymbol{v}-\dot{\boldsymbol{u}}) + \int_\Omega \boldsymbol{\mathcal{A}}\boldsymbol{\varepsilon}(\dot{\boldsymbol{u}}):\boldsymbol{\varepsilon}(\boldsymbol{v}-\dot{\boldsymbol{u}}) + \int_\Omega \boldsymbol{\mathcal{B}}\boldsymbol{\varepsilon}(\boldsymbol{u}):\boldsymbol{\varepsilon}(\boldsymbol{v}-\dot{\boldsymbol{u}}) + j(\boldsymbol{v},\alpha) \geq j(\dot{\boldsymbol{u}},\alpha) + \int_\Omega \boldsymbol{b}\cdot(\boldsymbol{v}-\dot{\boldsymbol{u}}) \quad \forall \boldsymbol{v}\in\mathcal{V}. \tag{17}$$

If we choose $\boldsymbol{v}$ as $\dot{\boldsymbol{u}}+\boldsymbol{w}$ with arbitrary $\boldsymbol{w}\in C_c^\infty(\Omega)$ then this tells us

$$\int_\Omega \rho\ddot{\boldsymbol{u}}\cdot\boldsymbol{w} + \int_\Omega \boldsymbol{\mathcal{A}}\boldsymbol{\varepsilon}(\dot{\boldsymbol{u}}):\boldsymbol{\varepsilon}(\boldsymbol{w}) + \int_\Omega \boldsymbol{\mathcal{B}}\boldsymbol{\varepsilon}(\boldsymbol{u}):\boldsymbol{\varepsilon}(\boldsymbol{w}) \geq \int_\Omega \boldsymbol{b}\cdot\boldsymbol{w},$$

so that we recover our original differential equation

$$\nabla\cdot[\boldsymbol{\mathcal{A}}\boldsymbol{\varepsilon}(\dot{\boldsymbol{u}}) + \boldsymbol{\mathcal{B}}\boldsymbol{\varepsilon}(\boldsymbol{u})] + \boldsymbol{b} = \rho\ddot{\boldsymbol{u}} \quad \text{in } \Omega. \tag{18}$$

We have already seen in the previous section that a solution to this equation satisfies

$$\int_\Omega \rho\ddot{\boldsymbol{u}}\cdot\boldsymbol{v} + \int_\Omega \boldsymbol{\mathcal{A}}\boldsymbol{\varepsilon}(\dot{\boldsymbol{u}}):\boldsymbol{\varepsilon}(\boldsymbol{v}) + \int_\Omega \boldsymbol{\mathcal{B}}\boldsymbol{\varepsilon}(\boldsymbol{u}):\boldsymbol{\varepsilon}(\boldsymbol{v}) = \int_{\Gamma_N} \boldsymbol{t}\cdot\boldsymbol{v} + \int_{\Gamma_C} \boldsymbol{\sigma}_t\cdot\boldsymbol{v} + \int_\Omega \boldsymbol{b}\cdot\boldsymbol{v} \quad \forall\boldsymbol{v}\in\mathcal{V};$$

this fact now allows us to extract a weak formulation of the non-essential boundary conditions from (17): We find

$$\int_{\Gamma_N} \boldsymbol{t}\cdot(\boldsymbol{v}-\dot{\boldsymbol{u}}) + \int_{\Gamma_C} \boldsymbol{\sigma}_t\cdot(\boldsymbol{v}-\dot{\boldsymbol{u}}) + j(\boldsymbol{v},\alpha) \geq j(\dot{\boldsymbol{u}},\alpha) \quad \forall\boldsymbol{v}\in\mathcal{V}. \tag{19}$$

To separate the conditions on Γ_N and Γ_C, we resort to an argument of density, namely proposition B.1: Since the surface traction $\boldsymbol{t}$ is square-integrable by assumption, (19) guarantees $\boldsymbol{t}=0$ on Γ_N. This leaves us with

$$\int_{\Gamma_C} \boldsymbol{\sigma}_t\cdot(\boldsymbol{v}-\dot{\boldsymbol{u}}) + j(\boldsymbol{v},\alpha) \geq j(\dot{\boldsymbol{u}},\alpha) \tag{20}$$

for any $\boldsymbol{v}\in\mathcal{V}$. If we could establish that (20) holds also for arbitrary $\boldsymbol{v}\in L^2(\Gamma_C)$ now, then this would certainly imply

$$-\boldsymbol{\sigma}_t \in \partial\big[\bar{\mu}(|\dot{\boldsymbol{u}}|,\alpha)|\sigma_n| + C|\dot{\boldsymbol{u}}|\big] \quad \text{almost everywhere in } \Gamma_C$$

as desired. Indeed, with a bit of work, the following can be shown.

4 The question when this is the case will not be answered here.

Proposition 2.2. *Let $\boldsymbol{v} \in L^2(\Gamma_C)^d$ and $\alpha \in \mathcal{X}$ be such that $j(\boldsymbol{v}, \alpha)$ is finite. Then we can find functions $\boldsymbol{v}_n \in \mathcal{V}$ that satisfy*

$$\boldsymbol{v}_n \to \boldsymbol{v} \text{ in } L^2(\Gamma_C)^d \quad \text{and} \quad j(\boldsymbol{v}_n, \alpha) \to j(\boldsymbol{v}, \alpha).$$

Proof. Step by step, we prove the following.[5]

- Without loss of generality, the function $\boldsymbol{v}$ can be assumed to lie in $L^\infty(\Gamma_C)$.
- We can find a sequence of functions $\boldsymbol{v}_n \in \gamma_C(\mathcal{V})$ with

$$\|\boldsymbol{v}_n\|_{L^\infty(\Gamma_C)} \leq \|\boldsymbol{v}\|_{L^\infty(\Gamma_C)} \tag{21}$$

  and $\boldsymbol{v}_n \to \boldsymbol{v}$ in $L^2(\Gamma_C)$ as $n \to \infty$.
- Such sequences satisfy $j(\boldsymbol{v}_n, \alpha) \to j(\boldsymbol{v}, \alpha)$.

Consider the family of truncation maps T_k on $\mathbb{R}^d$ defined by

$$T_k(\boldsymbol{w}) = \begin{cases} \frac{k}{|\boldsymbol{w}|}\boldsymbol{w} & \text{if } |\boldsymbol{w}| \geq k \\ \boldsymbol{w} & \text{otherwise} \end{cases}$$

for $k > 0$. By superposing T_k on $\boldsymbol{v}$ we get essentially bounded functions which converge to $\boldsymbol{v}$ in the sense of $L^2(\Gamma_C)$ as $k \to \infty$. Moreover, since $\bar{\mu}$ is nondecreasing, we have

$$j(T_k(\boldsymbol{v}), \alpha) \to j(\boldsymbol{v}, \alpha)$$

as a consequence of proposition B.10. Because it, therefore, suffices to approximate $T_k(\boldsymbol{v})$ for arbitrary $k > 0$, we may assume without loss of generality that $\boldsymbol{v}$ was truncated at the level k to begin with.
To construct approximations $\boldsymbol{v}_n$ of $\boldsymbol{v}$ now which satisfy (21), we find approximations that do not and truncate them.
Proposition B.1 gives us a sequence of functions $\boldsymbol{w}_n \in \gamma_C(\mathcal{V})$ with $\boldsymbol{w}_n \to \boldsymbol{v}$ in $L^2(\Gamma_C)^d$; their truncations $\boldsymbol{v}_n = T_k(\boldsymbol{w}_n)$ again lie in $\gamma_C(\mathcal{V})$ by proposition B.9 and also clearly satisfy

$$\boldsymbol{v}_n = T_k(\boldsymbol{w}_n) \to T_k(\boldsymbol{v}) = \boldsymbol{v} \text{ in } L^2(\Gamma_C) \quad \text{as } n \to \infty$$

since T_k is Lipschitz. Our claim thus follows once we prove

$$j(T_k(\boldsymbol{w}_n), \alpha) \to j(T_k(\boldsymbol{v}), \alpha) \quad \text{as } n \to \infty,$$

for which continuity of $j(T_k(\,\cdot\,), \alpha)$ as an operator from $L^2(\Gamma_C)$ to $L^1(\Gamma_C)$ is clearly sufficient. The right tool is of course proposition B.12, it only remains to be shown that $j(\boldsymbol{w}, \alpha)$ is finite for every $\boldsymbol{w} \in L^\infty(\Gamma_C)$. But

5 The key ideas for this proof have been kindly contributed by Donat Wegner.

this is a straightforward consequence of the assumptions (A1) and (A2): Observe only

$$\begin{aligned} j(\boldsymbol{w},\alpha) &= \int_{\Gamma_C} \bar{\mu}(|\boldsymbol{w}|,\alpha)|\sigma_n| + C|\boldsymbol{w}| \\ &\leq \int_{\Gamma_C} \bar{\mu}(W,\alpha)|\sigma_n| + CW \quad \text{with } W \coloneqq \|\boldsymbol{w}\|_{L^\infty(\Gamma_C)} \\ &\leq \int_{\Gamma_C} [\bar{\mu}(W,0) + L_\mu W|\alpha|]|\sigma_n| + CW < \infty. \end{aligned}$$

Now there is nothing left to show. □

3 TIME DISCRETISATION AND ANALYSIS

Assume now that the time interval $[0, T]$ is partitioned into N subintervals, *i.e.*

$$[0, T] = \bigcup_{i=1}^{N} [t_{i-1}, t_i]$$

with $0 = t_0 < \cdots < t_N = T$ and $\tau_i = t_i - t_{i-1}$ for $1 \leq i \leq N$. In what follows, we will derive a time-discrete approximation of problem 2.5, *i.e.* a sequence of problems with corresponding solutions α_n and u_n or $\dot{u}_n$, meant to approximate the time-continuous solution to the original problem at time t_n (if it exists).
Since the scheme will be of single-step type, so that any time step uses information from its immediate predecessor only, it is fully described by the transition from arbitrary initial data to a solution at time t_1. Consequently, we can focus on this case without any loss of generality and write τ in place of τ_1.
Recall that problem 2.2 and problem 2.4 can be written as

$$\dot{\alpha} = \dot{\alpha}(|\dot{\boldsymbol{u}}|, \alpha) \quad \text{on } \Gamma_C \tag{22}$$

and

$$\ell \in \mathcal{M}\ddot{\boldsymbol{u}} + \mathcal{C}\dot{\boldsymbol{u}} + \mathcal{K}\boldsymbol{u} + \partial j(\,\cdot\,, \alpha)(\dot{\boldsymbol{u}}), \tag{23}$$

respectively. To derive a time-discrete formulation, we follow a few simple steps.

- Require (23) to be satisfied (only) at time t_1, yielding

$$\ell_1 \in \mathcal{M}\ddot{\boldsymbol{u}}_1 + \mathcal{C}\dot{\boldsymbol{u}}_1 + \mathcal{K}\boldsymbol{u}_1 + \partial j(\,\cdot\,, \alpha_1)(\dot{\boldsymbol{u}}_1), \tag{24}$$

- Approximate $\dot{\boldsymbol{u}}$ on the time interval $(0, t_1]$ through the constant velocity $\dot{\boldsymbol{u}}_\lambda = \lambda\dot{\boldsymbol{u}}_0 + (1-\lambda)\dot{\boldsymbol{u}}_1$ with a fixed $\lambda \in [0, 1]$, so that we have

$$\dot{\alpha} = \dot{\alpha}(|\dot{\boldsymbol{u}}_\lambda|, \alpha). \tag{25}$$

- Apply a time stepping scheme to express $\ddot{\boldsymbol{u}}_1$ and $\boldsymbol{u}_1$ in terms of $\dot{\boldsymbol{u}}_1$, which gives

$$\ell_{1,0} \in \mathcal{Z}\dot{\boldsymbol{u}}_1 + \partial j(\,\cdot\,, \alpha_1)(\dot{\boldsymbol{u}}_1) \tag{26}$$

  with

$$\mathcal{Z} = \frac{\lambda_{\mathcal{M}}}{\tau}\mathcal{M} + \mathcal{C} + \frac{\tau}{\lambda_{\mathcal{K}}}\mathcal{K}$$

  and positive scalars $\lambda_{\mathcal{M}}$, $\lambda_{\mathcal{K}}$. The term $\ell_{1,0}$ here consists of ℓ_1 and forces arising from the previous time step.

Table 3.1: A selection of time stepping schemes.

Backward Euler scheme	
canonical presentation	$\boldsymbol{u}_1 = \boldsymbol{u}_0 + \tau\dot{\boldsymbol{u}}_1,\ \dot{\boldsymbol{u}}_1 = \dot{\boldsymbol{u}}_0 + \tau\ddot{\boldsymbol{u}}_1$
reformulation	$\boldsymbol{u}_1 = \boldsymbol{u}_0 + \tau\dot{\boldsymbol{u}}_1,\ \ddot{\boldsymbol{u}}_1 = \frac{\dot{\boldsymbol{u}}_1 - \dot{\boldsymbol{u}}_0}{\tau}$
resulting parameters	$\lambda_{\mathcal{K}} = 1,\ \lambda_{\mathcal{M}} = 1$
Newmark-β scheme with $\beta \in [0, 1/2]$	
canonical presentation[a]	$\boldsymbol{u}_1 = \boldsymbol{u}_0 + \tau\dot{\boldsymbol{u}}_0 + \frac{\tau^2}{2}\ddot{\boldsymbol{u}}_{2\beta}$ $\dot{\boldsymbol{u}}_1 = \dot{\boldsymbol{u}}_0 + \tau\frac{\ddot{\boldsymbol{u}}_1 + \ddot{\boldsymbol{u}}_0}{2}$
reformulation[b]	$\boldsymbol{u}_1 = \boldsymbol{u}_0 + \tau\dot{\boldsymbol{u}}_{2\beta} + \frac{\tau^2}{2}(1-4\beta)\ddot{\boldsymbol{u}}_0$ $\ddot{\boldsymbol{u}}_1 = 2\frac{\dot{\boldsymbol{u}}_1 - \dot{\boldsymbol{u}}_0}{\tau} - \ddot{\boldsymbol{u}}_0$
resulting parameters	$\lambda_{\mathcal{K}} = \frac{1}{2\beta},\ \lambda_{\mathcal{M}} = 2$

[a] with $\ddot{\boldsymbol{u}}_{2\beta} \coloneqq (1-2\beta)\ddot{\boldsymbol{u}}_0 + 2\beta\ddot{\boldsymbol{u}}_1$.
[b] with $\dot{\boldsymbol{u}}_{2\beta} \coloneqq (1-2\beta)\dot{\boldsymbol{u}}_0 + 2\beta\dot{\boldsymbol{u}}_1$.

The time stepping scheme is intentionally left unspecified at this point for the purpose of generality. A few options as well as the resulting values of $\lambda_{\mathcal{M}}$ and $\lambda_{\mathcal{K}}$ are provided in table 3.1.

In this manner, we obtain a coupled problem which is partly discrete. If we can establish that each subproblem has a unique solution for arbitrary data, we can also define corresponding solution operators $R\colon \alpha_1 \mapsto \dot{\boldsymbol{u}}_1$ and $S\colon \dot{\boldsymbol{u}}_1 \mapsto \alpha_1$. To solve the coupled problem is then to find a pair $(\dot{\boldsymbol{u}}_1, \alpha_1)$ such that $R\alpha_1 = \dot{\boldsymbol{u}}_1$ and $S\dot{\boldsymbol{u}}_1 = \alpha_1$, which means that α_1 is a fixed point of $S \circ R$ or equivalently that $\dot{\boldsymbol{u}}_1$ is a fixed point of $R \circ S$, as illustrated in figure 3.1.

$$\alpha_1 \underset{S}{\overset{R}{\rightleftarrows}} \dot{\boldsymbol{u}}_1$$

Figure 3.1: The fixed point problem for $R \circ S$ or $S \circ R$.

Whether such a fixed point exists is not immediately clear; there could also be more than just one. As is well known, Banach's fixed point theorem guarantees the existence of exactly one fixed point and provides a means to compute it. Since it can only be applied in rather restrictive circumstances, however, in this chapter, Schauder's non-constructive fixed point theorem, too, is used to prove existence of solutions.

3.1 FUNCTION SPACES

In problem 2.4, we have already specified that the solution $\boldsymbol{u}$ should satisfy $\dot{\boldsymbol{u}} \in \mathcal{V}$. In a time-discrete setting then, naturally, we look for a solution $\dot{\boldsymbol{u}}_1$ in the very same space. This approach will be justified by showing that it yields a unique solution. Before we can do that, however,

we need to find an appropriate space $\mathcal{X}$ for the state field α_1, so that we can define solution operators

$$S\colon \mathcal{V} \to \mathcal{X} \quad \text{and} \quad R\colon \mathcal{X} \to \mathcal{V}. \tag{27}$$

Not only does $\mathcal{X}$ need to be small enough for R to be well-defined and continuous, it should also be large enough to serve as a target space for S.
In what follows, the space $\mathcal{X}$ will be chosen as $L^2(\Gamma_C)$ for simplicity. The keen reader will notice, however, that it plays two separate roles: One that could be filled by a larger space and another which would also admit smaller spaces; both in accordance with proposition B.3.

3.2 SOLUTION OPERATORS

As outlined above, our time discretisation procedure yields two problems, one for the velocity $\dot{\boldsymbol{u}}_1$ and one for the state α_1. We first investigate the former, which can be stated as follows.

Problem 3.1. Assuming $\boldsymbol{b} \in L^2(\Omega)^d$, $\alpha_1 \in \mathcal{X}$, and $\boldsymbol{u}_0$, $\dot{\boldsymbol{u}}_0$, $\ddot{\boldsymbol{u}}_0 \in \mathcal{V}$, find $\dot{\boldsymbol{u}}_1 \in \mathcal{V}$ such that (26) is satisfied. The terms $\boldsymbol{u}_1$ and $\ddot{\boldsymbol{u}}_1$ can then be computed from $\dot{\boldsymbol{u}}_1$.

Since $\mathcal{Z}$ is a positive symmetric operator by construction and j is convex, by proposition B.7 this task is equivalent to the minimisation problem

$$\dot{\boldsymbol{u}}_1 = \arg\min_{\boldsymbol{v}} J_1(\boldsymbol{v}, \alpha_1)$$

with

$$J_1\colon \begin{cases} \mathcal{V} \times \mathcal{X} & \to \mathbb{R} \\ (\boldsymbol{v}, \alpha_1) & \mapsto \frac{1}{2}\langle \mathcal{Z}\boldsymbol{v}, \boldsymbol{v}\rangle + j(\boldsymbol{v}, \alpha_1) - \ell_{1,0}(\boldsymbol{v}). \end{cases}$$

Moreover, we have the following result.

Proposition 3.1. *Problem 3.1 has a unique solution for arbitrary $\alpha_1 \in \mathcal{X}$.*

Proof. By proposition B.8, we need only show the following properties of $J_1(\,\cdot\,, \alpha_1)$.

- The bilinear form $\boldsymbol{v} \mapsto \langle \mathcal{Z}\boldsymbol{v}, \boldsymbol{v}\rangle$ is continuous and coercive.
- The convex nonlinearity $j(\,\cdot\,, \alpha_1)$ is proper and lower semicontinuous.

The function $j(\,\cdot\,, \alpha_1)$ is clearly proper since it vanishes at zero, so that we only need to check lower semicontinuity. But since the functions $\bar{\mu}(|\,\cdot\,|, \alpha_1(\boldsymbol{x}))$ are continuous and nonnegative this immediately follows from proposition B.11.
Continuity of the bilinear form is also straightforward if we assume $\boldsymbol{\mathcal{B}}$, $\boldsymbol{\mathcal{A}}$, and ρ to be constant in space. For coercivity on $\mathcal{V}$ we can use Korn's inequality: If Γ_D has non-zero measure then both $\mathcal{K}$ and $\mathcal{C}$ are $\mathcal{V}$-coercive, see proposition B.2. □

As a consequence, we can indeed define a solution operator $R\colon \mathcal{X} \to \mathcal{V}$.

Proposition 3.2. *The operator*

$$R\colon \mathcal{X} \to \mathcal{V}, \quad \alpha \mapsto \dot{\boldsymbol{u}}_1 = \arg\min_{\boldsymbol{v}} J_1(\boldsymbol{v}, \alpha)$$

is well-defined and Lipschitz.

Proof. Let α, $\hat{\alpha} \in \mathcal{X}$ be arbitrary and write $\boldsymbol{v} = R(\alpha)$, $\hat{\boldsymbol{v}} = R(\hat{\alpha})$. By definition, this means

$$\begin{aligned}\langle \mathcal{Z}\boldsymbol{v}, \boldsymbol{w} - \boldsymbol{v}\rangle + j(\boldsymbol{w}, \alpha) &\geq j(\boldsymbol{v}, \alpha) + \ell_{1,0}(\boldsymbol{w} - \boldsymbol{v}),\\ \langle \mathcal{Z}\hat{\boldsymbol{v}}, \hat{\boldsymbol{w}} - \hat{\boldsymbol{v}}\rangle + j(\hat{\boldsymbol{w}}, \hat{\alpha}) &\geq j(\hat{\boldsymbol{v}}, \hat{\alpha}) + \ell_{1,0}(\hat{\boldsymbol{w}} - \hat{\boldsymbol{v}})\end{aligned}$$

for any $\boldsymbol{w}$, $\hat{\boldsymbol{w}} \in \mathcal{V}$; in particular, these inequalities hold for the choice $\boldsymbol{w} = \hat{\boldsymbol{v}}$, $\hat{\boldsymbol{w}} = \boldsymbol{v}$. After adding one to the other, we obtain

$$\begin{aligned}j(\hat{\boldsymbol{v}}, \alpha) + j(\boldsymbol{v}, \hat{\alpha}) - j(\boldsymbol{v}, \alpha) - j(\hat{\boldsymbol{v}}, \hat{\alpha}) &\geq \langle \mathcal{Z}(\hat{\boldsymbol{v}} - \boldsymbol{v}), \hat{\boldsymbol{v}} - \boldsymbol{v}\rangle\\ &\geq L_{\mathcal{Z}} \|\hat{\boldsymbol{v}} - \boldsymbol{v}\|_{\mathcal{V}}^2\end{aligned}$$

for a constant $L_{\mathcal{Z}} > 0$ by coercivity of $\mathcal{Z}$. This upper bound can in turn be bounded by means of assumption (A2), specifically

$$\begin{aligned}&j(\hat{\boldsymbol{v}}, \alpha) - j(\boldsymbol{v}, \alpha) + j(\boldsymbol{v}, \hat{\alpha}) - j(\hat{\boldsymbol{v}}, \hat{\alpha})\\ &\quad = |\sigma_n| \int_{\Gamma_C} \int_{|\boldsymbol{v}|}^{|\hat{\boldsymbol{v}}|} \mu(r, \alpha) - \mu(r, \hat{\alpha}) \,\mathrm{d}r\\ &\quad \leq |\sigma_n| \int_{\Gamma_C} L_\mu |\alpha - \hat{\alpha}| \cdot |\boldsymbol{v} - \hat{\boldsymbol{v}}|.\end{aligned}$$

We conclude

$$L_{\mathcal{Z}} \|\hat{\boldsymbol{v}} - \boldsymbol{v}\|_{\mathcal{V}}^2 \leq L_\mu |\sigma_n| \|\alpha - \hat{\alpha}\|_{\mathcal{X}} \|\gamma_C\| \|\boldsymbol{v} - \hat{\boldsymbol{v}}\|_{\mathcal{V}},$$

where $\|\gamma_C\|$ denotes the operator norm of the trace map $\gamma_C\colon \mathcal{V} \to \mathcal{X}^d$; the overall Lipschitz constant of R is given by

$$L_R \coloneqq \frac{L_\mu |\sigma_n| \|\gamma_C\|}{L_{\mathcal{Z}}}. \qquad \square$$

This completes the first half of the analysis of our discretisation procedure. Now on to the problem of solving (25), first pointwise. Since $\dot{\boldsymbol{u}}_\lambda$ is constant in time, this is an autonomous differential equation, and by assumption (A3) even a gradient flow, see appendix C. We can thus define flow maps $\Phi_t^{|\dot{\boldsymbol{u}}_\lambda|}$ for any $t \geq 0$ that allow us to phrase our problem as

Problem 3.2. Given $\alpha_0 \in \mathcal{X}$ and $\dot{\boldsymbol{u}}_0$, $\dot{\boldsymbol{u}}_1 \in \mathcal{V}$, compute $\alpha_1 = \Phi_\tau^{|\dot{\boldsymbol{u}}_\lambda|} \alpha_0$.

Formally, to define the solution operator S is now as simple as setting

$$S\colon \boldsymbol{w} \mapsto \Phi_\tau^{|\boldsymbol{w}_\lambda|}\alpha_0.$$

It remains to be shown, however, that S is well-defined as a map from $\mathcal{V}$ to $\mathcal{X}$. For this purpose, it is convenient to view S as a composition of four suboperators. In order of application, they are:

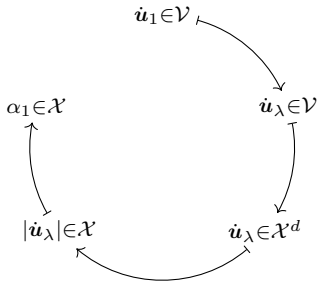

1. The map $\boldsymbol{v} \mapsto (1-\lambda)\dot{\boldsymbol{u}}_0 + \lambda\boldsymbol{v}$.
2. The trace map $\gamma_C\colon \mathcal{V} \to \mathcal{X}^d$.
3. The superposition operator corresponding to the Euclidean norm.
4. A superposition operator F induced by the map $(\boldsymbol{x}, V) \mapsto \Phi_\tau^V \alpha_0(\boldsymbol{x})$.

Of these operators, the first three are known to be well-defined and Lipschitz, only the superposition operator $F\colon \mathcal{X} \to \mathcal{X}$ requires further attention.[1]

If we assume that the function $\alpha(V, \cdot\,)$ has exactly one zero, denoted by $\alpha_{\mathrm{ss}}(V)$, then assumption (A3) tells us

$$\min\{\alpha, \alpha_{\mathrm{ss}}(V)\} \le \Phi_t^V \alpha \le \max\{\alpha, \alpha_{\mathrm{ss}}(V)\}$$

and in particular

$$|\Phi_t^V \alpha| \le |\alpha| + |\alpha_{\mathrm{ss}}(V)| \tag{28}$$

for any $t > 0$. To obtain a pointwise bound on F, it would thus suffice to bound $\alpha_{\mathrm{ss}}(V)$ in terms of the velocity V. For large velocities, this works quite well; the steady state $\alpha_{\mathrm{ss}}(V)$ will generally not remain bounded as V approaches zero, however, and possibly even cease to exist. This serves as the motivation for a two-part assumption on $\dot{\alpha}$.

(A4) For any positive velocity V, the function $\dot{\alpha}(V, \cdot\,)$ has exactly one zero, denoted by $\alpha_{\mathrm{ss}}(V)$, which satisfies

$$|\alpha_{\mathrm{ss}}(V)| \in \mathcal{O}(V) \quad \text{as } V \to \infty. \tag{29}$$

Moreover, there is a real-valued function η that satisfies

$$|\dot{\alpha}(V, \alpha)| \le \eta(W) \tag{30}$$

whenever $V \le W$ and $\dot{\alpha}(V, \alpha) \cdot \alpha \ge 0$.

The second half of assumption (A4) may seem a bit technical at first but the underlying idea is quite simple: Since we are only interested in advancing the time by a finite amount, if we had an α-independent bound on $\dot{\alpha}(V, \alpha)$ we could make use of the estimate

$$|\Phi_t^V \alpha| \le |\alpha| + t \max_{s \le t} |\dot{\alpha}(V, \Phi_s^V \alpha)|.$$

1 Even though Φ_τ^V is only defined for $V \ge 0$, we can treat F as an operator on the whole space $\mathcal{X}$ by extending it appropriately.

Typically, no such bound exists and α can evolve arbitrarily quickly even if V remains fixed. The problematic cases turn out to be harmless, however, since they have α evolve towards zero, which is to say

$$\dot{\alpha}(V, \alpha) \cdot \alpha \leq 0.$$

The following lemma formalises these observations.

Lemma 3.3. *Assumption (A4) implies that F is well-defined and continuous when combined with assumption (A3).*

Proof. In the following, we will show that (30) implies

$$|\Phi_t^V \alpha| \leq |\alpha| + t\eta(W) \quad \text{for } V \leq W,$$

thereby giving us a pointwise bound for small velocities; in combination with (28) and (29), this is clearly sufficient for F to map into $\mathcal{X}$, since it gives us a bound of the form

$$|\Phi_t^V \alpha| \leq C(t)[1 + V/V_*].$$

Continuity is then a consequence of proposition B.12. Let W, therefore, be an arbitrary velocity that satisfies $V \leq W$. By assumption (A3), this implies

$$|\Phi_t^V \alpha| \leq |\alpha| + t|\dot{\alpha}(V, \alpha)| \leq |\alpha| + t\eta(W)$$

as long as we have

$$\dot{\alpha}(V, \alpha) \cdot \alpha \geq 0. \tag{31}$$

If (31) is not satisfied, two cases can occur: Either the trajectory of α crosses the zero-line at a point $s \in [0, t]$, so that condition (30) applies to the flow starting at time s and we find

$$|\Phi_t^V \alpha| \leq (t - s)|\dot{\alpha}(V, \Phi_s^V \alpha)| \leq (t - s)\eta(W).$$

Or the trajectory does not cross the zero-line before time t, so that we even have

$$|\Phi_t^V \alpha| \leq |\alpha|. \qquad \square$$

Next we will show that this assumption covers the laws from section 1.2.

Proposition 3.4. *Both the ageing law (2) and the slip law (3) satisfy assumption (A4).*

Proof. Since the laws in question share the property

$$\alpha_{\text{ss}}(V) = \log(V_*/V),$$

the requirement (29) is clearly met. For the ageing law, furthermore, we have

$$|\dot{\alpha}(V, \alpha)| \leq \begin{cases} V_*/L & \text{whenever } \alpha,\ \dot{\alpha}(V, \alpha) \geq 0, \\ V/L & \text{whenever } \alpha,\ \dot{\alpha}(V, \alpha) \leq 0; \end{cases}$$

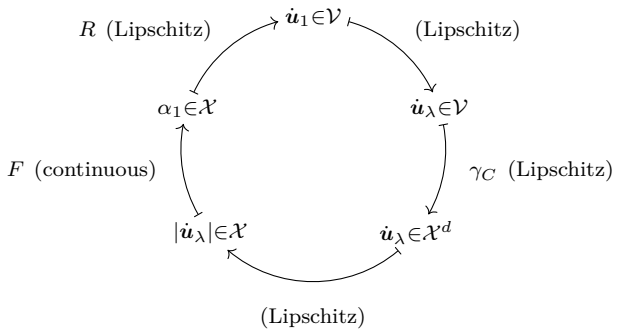

Figure 3.2: Details of the fixed point problem for $R \circ S$ or $S \circ R$.

similarly, the slip law is easily seen to satisfy

$$|\dot{\alpha}(V, \alpha)| \leq \frac{V}{L} \log \frac{V}{V_*}$$

whenever $\dot{\alpha}(V, \alpha) \cdot \alpha \geq 0$. Since these upper bounds are continuous functions of V, we can construct a nondecreasing bound η from the suprema on each interval $[0, W]$. □

To summarise, for a rate-and-state friction law that satisfies assumptions (A1) to (A4), our time-discrete coupled problem can be stated as follows.

Problem 3.3. Find a pair $(\dot{\boldsymbol{u}}_1, \alpha_1)$ such that $\dot{\boldsymbol{u}}_1$ solves problem 3.1 with respect to the state field α_1 and α_1 solves problem 3.2 with respect to the velocity field $\dot{\boldsymbol{u}}_1$.
Equivalently, find a fixed point of either $R \circ S$ or $S \circ R$ whose suboperators are shown in figure 3.2.

3.3 EXISTENCE AND UNIQUENESS OF SOLUTIONS

If the operator $R \circ S$ is a contraction on $\mathcal{V}$, then by proposition B.5, problem 3.3 must have a unique solution.
We have learnt from proposition 3.2 that R is Lipschitz with the constant L_R; in the presence of viscosity, furthermore, the constant $L_{\mathcal{Z}}$ and thus L_R can be chosen independently of τ; what we need to investigate further is F: In order for $R \circ S$ to have an arbitrarily small Lipschitz constant for small enough τ, it suffices for F to have this property. To that end, we make the following assumption, which renders assumption (A4) unnecessary.

(A5) The function $\dot{\alpha}$ is uniformly Lipschitz in its second argument; in other words, we have

$$|\dot{\alpha}(V, \alpha) - \dot{\alpha}(W, \alpha)| \leq L_{\dot{\alpha}} |V - W|$$

for any α and V, $W \geq 0$.

Proposition 3.5. *Any law that meets assumptions (A3) and (A5) also satisfies*

$$|\Phi_t^V \alpha - \Phi_t^W \alpha| \leq t L_{\dot\alpha} |V - W| \tag{32}$$

for any $t > 0$. In particular, for any $\alpha_0 \in \mathcal{X}$, the operator F corresponding to such a law is Lipschitz with respect to the constant $tL_{\dot\alpha}$.

Proof. Let V and W be two different velocities and observe that we can find a nonpositive function κ that satisfies

$$\begin{aligned}
&\frac{\mathrm{d}}{\mathrm{d}t}(\Phi_t^V \alpha - \Phi_t^W \alpha) \\
&\quad = \dot\alpha(V, \Phi_t^V \alpha) - \dot\alpha(W, \Phi_t^V \alpha) + \dot\alpha(W, \Phi_t^V \alpha) - \dot\alpha(W, \Phi_t^W \alpha) \\
&\quad = \dot\alpha(V, \Phi_t^V \alpha) - \dot\alpha(W, \Phi_t^V \alpha) + \kappa(t)\Big(\Phi_t^V \alpha - \Phi_t^W\Big) \\
&\quad \leq L_{\dot\alpha} |V - W| + \kappa(t)\Big(\Phi_t^V \alpha - \Phi_t^W\Big)
\end{aligned}$$

by virtue of assumption (A3). The claim is now a consequence of proposition B.4. □

The ageing law (2) clearly satisfies assumption (A5).

Let us also take a look at the dependence of $\dot{\boldsymbol{u}}_1$ and α_1 on the initial conditions. By assumption (A3), the flow Φ_t is nonexpansive for any $t \geq 0$, the operator S is thus nonexpansive with respect to the initial datum α_0. Similarly, if we consider two sets of initial data for problem 3.1 with corresponding right-hand sides $\ell_{1,0}$ and $\tilde\ell_{1,0}$ as well as solution operators R and $\tilde R$, then an easy calculation shows

$$\|R\alpha - \tilde R\alpha\| \leq \frac{\|\ell_{1,0} - \tilde\ell_{1,0}\|}{L_{\mathcal{Z}}}.$$

In other words, the operator R is Lipschitz with respect to its initial conditions. This Lipschitz dependence carries over from R and S to the fixed point of their composition and thus to the solution of problem 3.3. To see that this is so,[2] we write

$$\lim_{n\to\infty} (R \circ S)^n \boldsymbol{v} \quad \text{and} \quad \lim_{n\to\infty} (\tilde R \circ S)^n \boldsymbol{v} \quad \text{with arbitrary } \boldsymbol{v} \in \mathcal{V}$$

for the two solutions corresponding to the aforementioned initial data and pass to the limit in the upper bounds

$$\begin{aligned}
&\Big\|(R \circ S)^n \boldsymbol{v} - (\tilde R \circ S)^n \boldsymbol{v}\Big\| \\
&\quad = \left\|\sum_{k=0}^{n-1} [(R \circ S)^{n-k} - (R \circ S)^{n-k-1} \circ (\tilde R \circ S)][(\tilde R \circ S)^k \boldsymbol{v}]\right\| \\
&\quad \leq \sum_{k=0}^{n-1} (L_R L_S)^{n-k-1} \Big\|[(R \circ S) - (\tilde R \circ S)][(\tilde R \circ S)^k \boldsymbol{v}]\Big\| \\
&\quad \leq \sum_{k=0}^{n-1} (L_R L_S)^{n-k-1} \frac{\|\ell_{1,0} - \tilde\ell_{1,0}\|}{L_{\mathcal{Z}}}.
\end{aligned}$$

2 The following calculation only varies the initial data for the operator R, not S. The case of variable α_0 is completely analogous.

In summary, we have shown the following in this section.

Proposition 3.6. *In the presence of viscosity, if a rate-and-state law satisfies assumptions (A1) to (A3) and (A5), then there is a time step size $\tau_{\max} > 0$, such that problem 3.3 has a unique solution for any time steps size $\tau \leq \tau_{\max}$. In such cases, moreover, the dependence of the solution $(\dot{\boldsymbol{u}}_1, \alpha_1)$ on the initial data is Lipschitz and the term $(R \circ S)^n \boldsymbol{v}$ converges to $\dot{\boldsymbol{u}}_1$ as $n \to \infty$, regardless of the choice of $\boldsymbol{v} \in \mathcal{V}$.*

It should be noted $\tau_{\max}$ does not depend on the initial data of problem 3.3; in other words, the corresponding statements can also be made for the next time step, without changing $\tau_{\max}$.

3.4 EXISTENCE IN A MORE GENERAL SETTING

Unfortunately, the operator F corresponding to the slip law (3) is not Lipschitz. This prompts us to leave the world of contractions and consider different fixed point sources. Indeed, since the trace map $\gamma_C \colon \mathcal{V} \to \mathcal{X}^d$ is compact by proposition B.3, so is $R \circ S$. What separates us from an application of Schauder's fixed point theorem is knowledge of a bounded convex set in $\mathcal{V}$ which is invariant under $R \circ S$.
In this section, therefore, we will show that for any law that meets assumptions (A1) to (A3) as well as a strengthening of assumption (A4), the operator $R \circ S$ maps sufficiently large balls in $\mathcal{V}$ into themselves.

A sufficient strengthening is the following, which is clearly satisfied by both the ageing law (2) and the slip law (3).

(A6) For any positive velocity V, the function $\dot{\alpha}(V, \cdot\,)$ has exactly one zero, denoted by $\alpha_{\mathrm{ss}}(V)$, which satisfies

$$|\alpha_{\mathrm{ss}}(V)| \in \mathcal{O}(\sqrt{V}) \quad \text{as } V \to \infty.$$

Moreover, there is a real-valued function η that satisfies

$$|\dot{\alpha}(V, \alpha)| \leq \eta(W) \tag{33}$$

whenever $V \leq W$ and $\dot{\alpha}(V, \alpha) \cdot \alpha \geq 0$.

By the argument already employed in the proof of lemma 3.3, this gives us a bound of the form

$$|\Phi_t^V \alpha| \leq |\alpha| + C(t)(1 + \sqrt{V/V_*}).$$

The task is now to turn this knowledge about pointwise growth into a bound on the growth of $\|FV\|$ as $\|V\| \to \infty$ in $\mathcal{X}$.

Proposition 3.7. *Under assumptions (A3) and (A6), the operator F satisfies*

$$\|FV\|_{\mathcal{X}} \in \mathcal{O}(\sqrt{\|V\|_{\mathcal{X}}}) \quad \text{as } \|V\|_{\mathcal{X}} \to \infty \text{ in } \mathcal{X}.$$

In particular, under the additional assumptions (A1) and (A2), the operator $R \circ S$ is a self-map on sufficiently large balls in $\mathcal{V}$.

Proof. Note that we have

$$\|\sqrt{V/V_*}\|_{\mathcal{X}} = \left(\int_{\Gamma_C} V/V_*\right)^{1/2} \leq C(\Gamma_C)\|V/V_*\|_{\mathcal{X}}^{1/2}$$

and thus

$$\|\Phi_t^V \alpha_0\|_{\mathcal{X}} \leq \|\alpha_0\|_{\mathcal{X}} + C(t)\Big(\|1\|_{\mathcal{X}} + C(\Gamma_C)\|V/V_*\|_{\mathcal{X}}^{1/2}\Big).$$

Since the other suboperators of S are Lipschitz and so is R, it follows that $R \circ S$ has the same asymptotic growth as F. □

Corollary 3.8. *For any law that satisfies assumptions (A1) to (A3) and (A6), problem 3.3 has a (potentially non-unique) solution.*

Proof. This is a consequence of proposition B.6. □

While we do learn only about existence from this result, it is quite general: Not only does it cover the slip law (3), it also works in the purely elastic case, *i.e.* in the absence of viscosity, and does not make any assumptions on the time step size τ.

4 SPATIAL DISCRETISATION

Assume now that the domain Ω is covered by a conforming grid G. Write $(\lambda_i)_{1\leq i\leq K}$ for the nodal basis as well as $\mathcal{S}\subset\mathcal{V}$ for the space of linear finite element functions on G which satisfy the boundary conditions (9) and (11). To obtain a fully discrete approximation of problem 3.3, we take the following steps.

- Repose problem 3.1 over the space $\mathcal{S}$. This has us find a coefficient vector $\underline{\dot{\boldsymbol{u}}}$ in the space

$$\underline{\mathcal{S}} = \left\{ \underline{\boldsymbol{v}} \in \mathbb{R}^{K\times d} \colon \sum_i \lambda^i \underline{\boldsymbol{v}}^i \in \mathcal{S} \right\}$$

  such that the discrete functional $\underline{J}(\,\cdot\,,\alpha_1)$ given by

$$\begin{aligned}\underline{J}(\underline{\boldsymbol{v}},\alpha_1) &= J_1\Big(\sum_i \lambda^i \underline{\boldsymbol{v}}^i, \alpha_1\Big)\\ &= \frac{1}{2}\sum_{i,k}\langle \underline{\mathcal{Z}}^{i,k}\underline{\boldsymbol{v}}^k, \underline{\boldsymbol{v}}^i\rangle - \sum_i \langle \underline{\boldsymbol{b}}^i, \underline{\boldsymbol{v}}^i\rangle\\ &\quad + \int_{\Gamma_C} \bar{\mu}\Big(\Big|\sum_i \lambda^i \underline{\boldsymbol{v}}^i\Big|, \alpha_1\Big)|\sigma_n| + C\Big|\sum_i \lambda^i \underline{\boldsymbol{v}}^i\Big|\end{aligned}$$

  with

$$\underline{\mathcal{Z}}^{i,k}_{j,l} = \langle \mathcal{Z}(\lambda^k \underline{\boldsymbol{e}}^l), \lambda^i \underline{\boldsymbol{e}}^j\rangle, \quad \underline{\boldsymbol{b}}^i_j = \ell_{1,0}(\lambda^i \underline{\boldsymbol{e}}^j), \quad \text{and} \quad \underline{\boldsymbol{e}}^i_j = \delta_{ij}$$

  is minimised.[1]

- Require the condition $\alpha_1 = \Phi_\tau^{|\dot{\boldsymbol{u}}_\lambda|}\alpha_0$ from problem 3.2 to hold only at points $\boldsymbol{x}_j$ which correspond to a grid node on the boundary Γ_C, and admit only solutions from the space $\gamma_C(\mathcal{S})\subset\mathcal{X}$, leaving us with following task.
  Problem 4.1. Find $\underline{\alpha}\in\mathbb{R}^K$ such that

$$\underline{\alpha}^j = \alpha(\boldsymbol{x}_j) = \begin{cases} \Phi_\tau^{|\dot{\boldsymbol{u}}_\lambda(\boldsymbol{x}_j)|}\alpha_0(\boldsymbol{x}_j) & \text{if } \boldsymbol{x}_j \in \Gamma_C,\\ 0 & \text{otherwise.}\end{cases} \tag{34}$$

  Note that we assume the initial data $\dot{\boldsymbol{u}}_0$ and α_0 to have well-defined point values here. This is certainly justified in the special case $\dot{\boldsymbol{u}}_0\in\mathcal{S}$, $\alpha_0\in\gamma_C(\mathcal{S})$; in the general case, we need to use an approximation.

1 The discrete quantities introduced here are time step specific, even though they are not explicitly labelled as such.

- Apply mass lumping to the nonlinear part of $\underline{J}$ to obtain the discrete approximation $\underline{\tilde{J}}$ given by

$$\underline{\tilde{J}}(\underline{\boldsymbol{v}}, \underline{\alpha}) = \sum_i \left(\frac{1}{2} \sum_k \langle \underline{\mathcal{Z}}^{i,k} \underline{\boldsymbol{v}}^k, \underline{\boldsymbol{v}}^i \rangle - \langle \underline{\boldsymbol{b}}^i, \underline{\boldsymbol{v}}^i \rangle + \psi^i(\underline{\boldsymbol{v}}^i, \underline{\alpha}^i) \right),$$

with

$$\psi^i(\underline{\boldsymbol{v}}^i, \underline{\alpha}^i) = [\bar{\mu}(|\underline{\boldsymbol{v}}^i|, \underline{\alpha}^i)|\sigma_n| + C|\underline{\boldsymbol{v}}^i|] \int_{\Gamma_C} \lambda^i.$$

Problem 4.2. Find $\dot{\underline{\boldsymbol{u}}} \in \underline{\mathcal{S}}$ that minimises $\underline{\tilde{J}}(\,\cdot\,, \underline{\alpha})$.

The fully discrete coupled problem is thus

Problem 4.3. Find a pair $(\dot{\underline{\boldsymbol{u}}}, \underline{\alpha}) \in \underline{\mathcal{S}} \times \mathbb{R}^K$ such that $\dot{\underline{\boldsymbol{u}}}$ solves problem 4.2 and $\underline{\alpha}$ solves problem 4.1.

As is easily checked, the results on existence and uniqueness of solutions for the spatially continuous problem 3.3 from the previous section carry over to the fully discrete setting. We know that there has to be a solution and that — at least if we use the ageing law and sufficiently small a time step — the coupling can be resolved through a simple fixed point iteration. What we have yet to answer is how the discrete problems 4.1 and 4.2 can be handled.

Problem 4.1 is certainly not an issue: In many situations, the solution can be computed analytically, *e.g.* for the ageing law (2) or the slip law (3). If this were not the case, a time stepping scheme could be used; the gradient flow structure implies that the backward Euler scheme would be well-behaved, for example.
To solve problem 4.2, we can use methods of convex minimisation. Let us first take a look at the block Gauß-Seidel scheme, *i.e.* successive minimisation at each grid node. While generally too slow to serve as the sole solver of a reasonably-sized problem, this method continues to be useful due to its extensibility: A block problem need not be solved accurately as long as enough descent is guaranteed; in addition, the scheme can be interspersed with iterations of another (potentially considerably faster but not necessarily convergent) energy-decreasing method, without putting convergence in jeopardy.
This observation, which is central to the idea behind so-called monotone multigrid methods, is employed here, too, through TNNMG, the *truncated nonsmooth Newton multigrid method*; see [6]
The application is straightforward and not central to this work, however, so that it is for the most part not discussed. One detail that does deserve attention is the approximate solution of block problems arising from successive nodewise minimisation of $\underline{\tilde{J}}$: At each node m, we need to find

$$\operatorname*{arg\,min}_{\Delta \underline{\boldsymbol{v}} \in \underline{\mathcal{S}}_m} \underline{\tilde{J}}(\underline{\boldsymbol{v}} + \Delta \underline{\boldsymbol{v}}, \underline{\alpha}) \quad \text{with} \quad \underline{\mathcal{S}}_m = \{\underline{\boldsymbol{w}} \in \underline{\mathcal{S}} \colon \underline{\boldsymbol{w}}^i = 0 \text{ if } i \neq m\}$$

with given $\underline{\boldsymbol{v}}$. In terms of the correction $\Delta\underline{\boldsymbol{v}}$, that is tantamount to minimising

$$\tilde{\underline{J}}(\underline{\boldsymbol{v}}+\Delta\underline{\boldsymbol{v}},\underline{\alpha}) = \frac{1}{2}\sum_{i,k}\langle \underline{\mathcal{Z}}^{i,k}(\underline{\boldsymbol{v}}+\Delta\underline{\boldsymbol{v}})^k, (\underline{\boldsymbol{v}}+\Delta\underline{\boldsymbol{v}})^i\rangle \\ - \sum_i \langle \underline{\boldsymbol{b}}^i, (\underline{\boldsymbol{v}}+\Delta\underline{\boldsymbol{v}})^i\rangle + \sum_i \psi^i((\underline{\boldsymbol{v}}+\Delta\underline{\boldsymbol{v}})^i, \underline{\alpha}^i)$$

or equivalently

$$\tilde{\underline{J}}^m(\Delta\underline{\boldsymbol{v}}^m) = \frac{1}{2}\langle \underline{\mathcal{Z}}^{m,m}\Delta\underline{\boldsymbol{v}}^m, \Delta\underline{\boldsymbol{v}}^m\rangle - \langle \underline{\boldsymbol{r}}^m, \Delta\underline{\boldsymbol{v}}^m\rangle + \psi^m(\underline{\boldsymbol{v}}^m+\Delta\underline{\boldsymbol{v}}^m, \underline{\alpha}^m)$$

with $\underline{\boldsymbol{r}}^m = \underline{\boldsymbol{b}}^m - \sum_i \underline{\mathcal{Z}}^{i,m}\underline{\boldsymbol{v}}^i$.
While these problems are very low-dimensional, they are still nonsmooth: The Euclidean norm not differentiable at the origin, and $\mu(\,\cdot\,,\alpha)$ is not required to be continuous. In order to solve them within a reasonable time-frame, we need to put their structure to use.
Following [7], we compute the largest eigenvalue σ^m of $\underline{\mathcal{Z}}^{m,m}$ and consider the *model* $\underline{I}^m$ given by

$$\begin{aligned}\underline{I}^m(\Delta\underline{\boldsymbol{v}}^m) &= \frac{\sigma^m}{2}|\Delta\underline{\boldsymbol{v}}^m|^2 - \langle \underline{\boldsymbol{r}}^m, \Delta\underline{\boldsymbol{v}}^m\rangle + \psi^m(\underline{\boldsymbol{v}}^m+\Delta\underline{\boldsymbol{v}}^m, \underline{\alpha}^m)\\ &= \frac{\sigma^m}{2}|\underline{\boldsymbol{v}}^m+\Delta\underline{\boldsymbol{v}}^m|^2 - \langle \tilde{\underline{\boldsymbol{r}}}^m, \underline{\boldsymbol{v}}^m+\Delta\underline{\boldsymbol{v}}^m\rangle\\ &\quad + \psi^m(\underline{\boldsymbol{v}}^m+\Delta\underline{\boldsymbol{v}}^m, \underline{\alpha}^m) + \text{const.}\end{aligned}$$

with $\tilde{\underline{\boldsymbol{r}}}^m = \underline{\boldsymbol{r}}^m + \sigma^m\underline{\boldsymbol{v}}^m$. Let us record some of its properties, most of which are easily verified.

- The model is first-order accurate, which is to say $\tilde{\underline{J}}^m(0) = \underline{I}^m(0)$ and $\partial\tilde{\underline{J}}^m(0) = \partial\underline{I}^m(0)$. Moreover, we have $\tilde{\underline{J}}^m \le \underline{I}^m$, so that the model *dominates* $\tilde{\underline{J}}^m$.
- Consequently, whenever $\Delta\underline{\boldsymbol{v}}^m$ is a descent direction of $\underline{I}^m$, then it also generates descent for $\tilde{\underline{J}}^m$, since then
$$\tilde{\underline{J}}^m(\Delta\underline{\boldsymbol{v}}^m) \le \underline{I}^m(\Delta\underline{\boldsymbol{v}}^m) < \underline{I}^m(0) = \tilde{\underline{J}}^m(0).$$
- The model has a unique minimiser, which is the solution of a one-dimensional problem. Indeed, since the subdifferential of the function $\psi^m(\,\cdot\,,\underline{\alpha}^m)$ at any point $\boldsymbol{\omega}$ is made up exclusively of multiples of $\boldsymbol{\omega}$, the minimiser of the function
$$\boldsymbol{\omega} \mapsto \frac{\sigma^m}{2}|\boldsymbol{\omega}|^2 - \langle \tilde{\underline{\boldsymbol{r}}}^m, \boldsymbol{\omega}\rangle + \psi^m(\boldsymbol{\omega}, \underline{\alpha}^m)$$
must be a multiple of $\tilde{\underline{\boldsymbol{r}}}^m$.
- Finally, the descent generated by the minimiser of $\underline{I}^m$ is significant for $\tilde{\underline{J}}^m$ in that even an inexact Gauß-Seidel iteration that minimises $\underline{I}^m$ instead of $\tilde{\underline{J}}^m$ converges (to the solution of problem 4.2).

At each node, this strategy thus requires no more than the solution of a problem in one dimension.[2] Such problems can be solved through bisection.

2 Since each block $\underline{\underline{\mathcal{Z}}}^{m,m}$ is only two- or three-dimensional, its eigenvalues are easily found.

5 APPLICATIONS

In their recent works [15, 16], Rosenau et al. report on laboratory experiments for an analogue subduction zone model.[1] Their setup consists of an inclined, primarily granular wedge that is positioned on top of a conveyor plate; figure 5.1 shows a sketch.
Over the course of the experiment, the wedge is pushed against a rigid back and thus compressed, leading to observable slip instabilities at its base, which resemble so-called megathrust earthquakes.

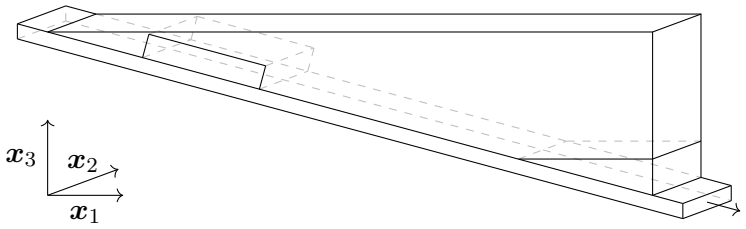

Figure 5.1: Experimental setup. Not shown are the glass sides (front and rear) and the rigid backstop (right).

This analogue model is from a numerical point of view pleasanter than a real subduction zone, primarily for two reasons: The wedge is rather thin so that it can be treated as essentially two-dimensional, and the temporal scale separation between stress build-up and stress release is less pronounced.
If we apply our numerical model and algorithm to this setting, we obtain problems which can be solved in a single-threaded environment within a reasonable time frame; a three-dimensional real-world scale problem, in contrast, would require a parallel solver and access to a supercomputer.

The following sections are thus dedicated to results from simulations based on the analogue model. These results can unfortunately not be expected to agree with the laboratory measurements exactly since the experimental setup violates some of the assumptions of our model: most prominently, the wedge undergoes finite, plastic deformation and at least near its shallow end, the normal stress cannot be expected to stay constant. Despite these concerns, the agreement between experiment and simulation turns out to be satisfactory.

1 In analogue modelling, laboratory experiments for real-world phenomena are carried out with materials whose behaviour on the laboratory scale is found to be analogous to that of real-world materials on the real-world scale.

5.1 PROBLEM DESCRIPTION

The wedge measures 10 cm in depth, 1 m in length and 27 cm in height. Since its top and rightmost face are perfectly horizontal and vertical, respectively, this gives it a dipping angle of approximately 15°.
Its lower 6 cm are made up of a viscous fluid; further up the base, a block of rate-weakening material serves as the seismogenic zone. This block is 4 cm thick, measures 20 cm along the base, and ends 35 cm from the shallow end, or *trench*, measured along the surface. The remaining material is homogeneous and strongly rate-strengthening.
The conveyor plate, finally, is operated at a constant speed, corresponding to the tectonic plate convergence velocity in nature.

5.2 MATHEMATICAL MODELLING

Naturally, we are interested in the velocity field of the wedge, which can be assumed to undergo rate-and-state friction. Since the state field is not known, this leaves us with a problem of essentially the same type as problem 2.3.
To see that this is so, let us first choose another frame of reference. We want a rigid foundation that is completely static; clearly, then, we should view the problem from the conveyor plate's perspective shown in figure 5.2: From this point of view, it is the backstop that moves at a prescribed pace and the slip rate that occurs in the rate-and-state formulation is simply the velocity relative to this frame.

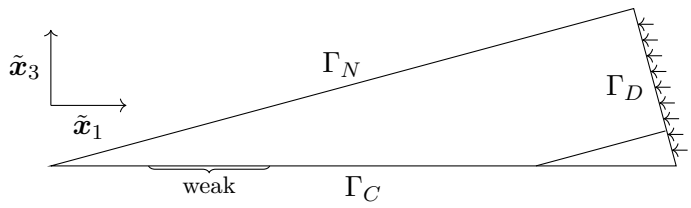

Figure 5.2: Rotated and simplified, two-dimensional computational domain.

Since the wedge is homogeneous in the direction of $\boldsymbol{x}_2$, and also rather thin, it is not unreasonable to neglect variations in the corresponding coordinate and use a two-dimensional model.
As a final step, we need to assume the rate-weakening region to be of infinitesimal height, so that it has an effect on the values of a and b only.[2]

Whenever possible, we should choose the parameters in the numerical calculation close to the experiment. Most are known, to an order of magnitude at least; some that we have little knowledge about are the

2 The agreement between both problems is still not perfect: On Γ_D, here, we prescribe the velocity in direction $\tilde{\boldsymbol{x}}_1$ only. Some of the parameters are also heterogeneous that were previously assumed uniform in space. These differences are only of technical nature, however.

elastic and viscous properties of the material which makes up most of the wedge. The bulk modulus has been determined to be of the order of 0.1 MPa but neither Poisson's ratio nor the viscosity have been investigated. Preliminary sensitivity studies suggest a choice of equivalent parameters given in table 5.1.

Table 5.1: Material parameters.

Parameter		Unit	Simulation	Experiment
Gravitational acceleration		m/s	9.81	9.81
Bulk modulus		MPa	0.05	0.10
Poisson's ratio			0.3	unknown
Viscosity, upper region		kPa s	1	unknown
Viscosity, lower region		kPa s	10	10
Mass density ρ, upper region		kg/m^3	900	900
Mass density ρ, lower region		kg/m^3	1000	1000
Cohesion C		Pa	10	10
Friction	L	µm	25	unknown
	V_*	µm/s	50	50
	μ_*		0.7	variable[a]
	a, unstable		0.002	unknown[b]
	a, stable		0.025	unknown[c]
	$b-a$, unstable		0.012	0.015
	$b-a$, stable		−0.020	variable[d]
Conveyor plate velocity		µm/s	50	50
Experiment duration T		s	1800	1000

[a] From 0.7 in the bulk to 0.8 in the seismogenic zone.
[b] Known upper bound: 0.002 (Rosenau, personal communication).
[c] Order of magnitude: 0.010 to 0.020 (Rosenau, personal communication).
[d] Order of magnitude: −0.020 to −0.010.

At time zero, the body is static and its displacement is governed by gravitational forces alone, which is to say

$$\mathcal{K}\boldsymbol{u}(0) = \ell(0).$$

In deviation from the experiment, so as not to introduce any unnecessary instability into the system, it seems reasonable to start from the uniform velocity field $\dot{\boldsymbol{u}}(0) = 0$, followed by a quick but smooth transition to the regime of constant shearing, or *loading*. To that end, I have chosen to let the Dirichlet condition on Γ_D in direction of $\tilde{\boldsymbol{x}}_1$ equal the plate convergence velocity only up to a factor of $\zeta(10t/T)$ for $t \leq T/10$, where the function ζ provides a smooth zero-to-one transition and is given by

$$\zeta(s) = \frac{1 - \cos(\pi \cdot s)}{2}$$

for $s \in [0, 1]$.

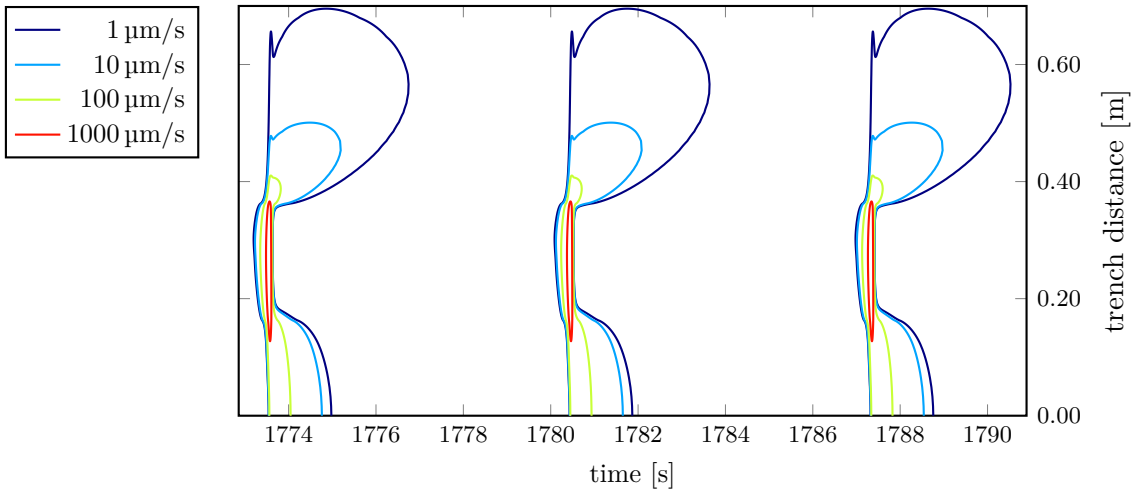

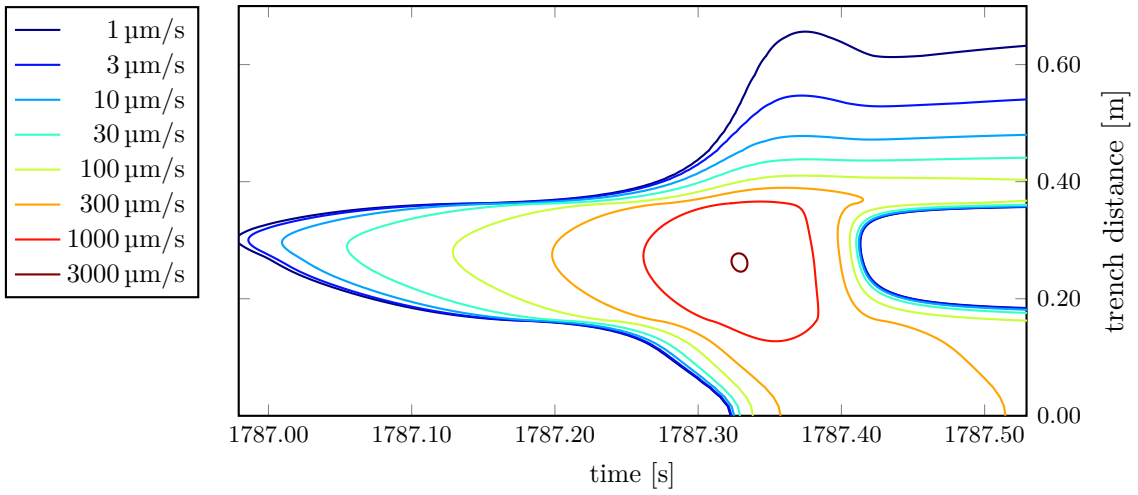

(a) The basal slip rate relative to plate convergence.

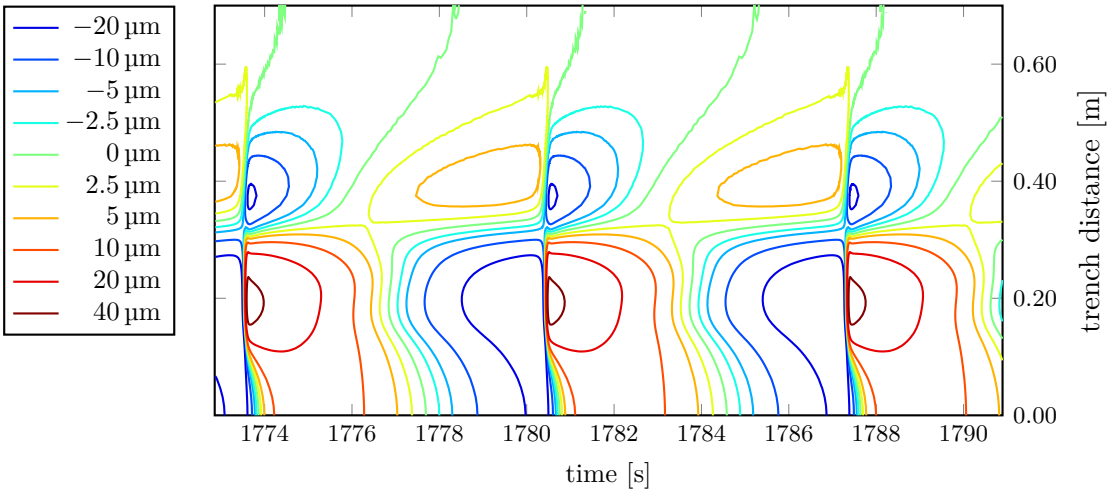

(b) Vertical surface displacement relative to a time average.

Figure 5.3: Basal slip rate and surface displacement. Simulation based on the ageing law.

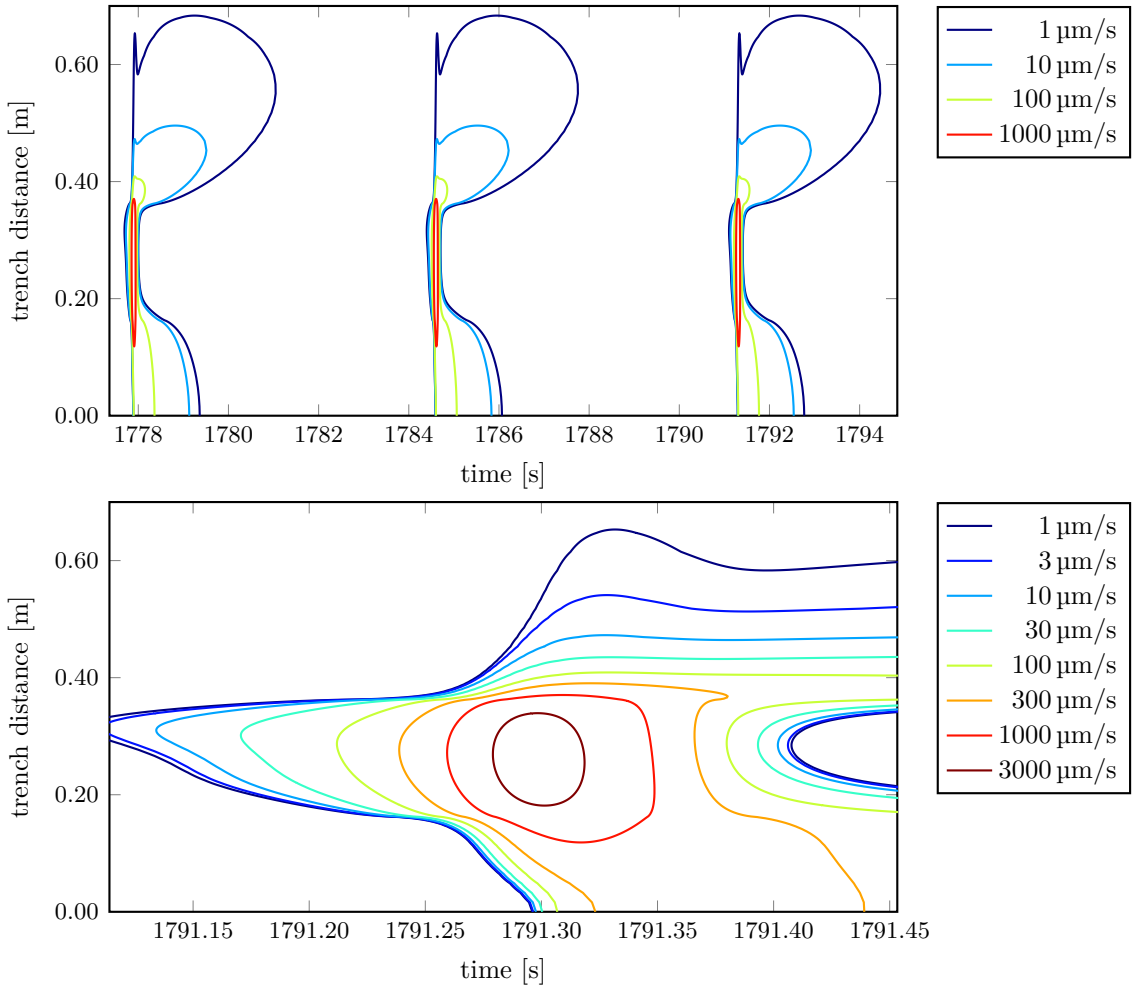

(a) The basal slip rate relative to plate convergence.

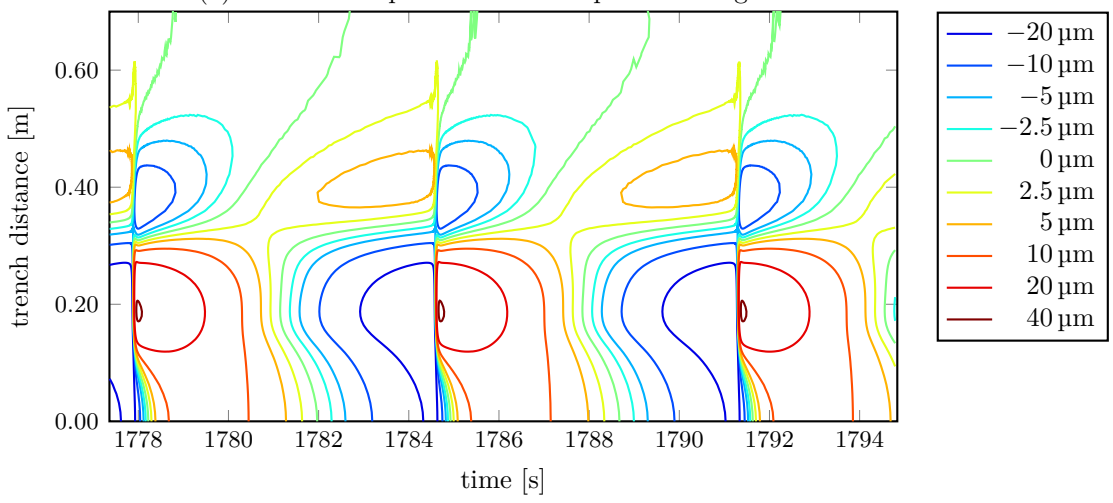

(b) Vertical surface displacement relative to a time average.

Figure 5.4: Basal slip rate and surface displacement. Simulation based on the slip law.

5.3 RESULTS

In both experiment and simulation, the wedge undergoes a quasistatic loading phase, followed by a sequence of seismic cycles. Each cycle consists of a seismic slip event, which is preceded by a comparatively long phase of interseismic stress build-up and followed by a post-seismic phase, during which afterslip occurs.[3]

These observations can be made in simulations based on either the ageing law (2) or the slip law (3). Let us first consider the former. Numerical details can be found in appendix A, it suffices to note here that the resolution has been found high enough both in time and space for numerical errors not to play a role.

In figure 5.3a, we see the spatiotemporal evolution of the basal sliding velocity over the course of a few seismic cycles as well as a zoom into a coseismic phase.

We can clearly see how rupture nucleates in the interior of this region. The sliding velocity grows exponentially here, until it peaks and decreases even more quickly than it rose. In the neighbouring regions, meanwhile, velocities see moderate growth, increase only after a time delay, and decrease so slowly thereafter, that nonneglible slip can be observed even when the seismogenic zone has long settled; this is the aforementioned *afterslip*.

Figure 5.3b show the same time-frame from a different perspective: During the interseismic period, material sticks to the conveyor plate, is transported towards and piled up against the backstop, and only in the coseismic period returned to its origin; hence we see an abrupt alternation of subsidence and uplift along the surface of the wedge.

Figures 5.4a and 5.4b show the corresponding contours over a similar time-frame for a simulation based on the slip law. The differences are purely quantitative: basal sliding accelerates more quickly and decelerates less quickly; the surface sees subsidence and uplift in exactly the same manner, only at a slightly lower intensity.

5.4 COMPARISON OF SIMULATION AND EXPERIMENT

Of the many quantities that can be used to describe the dynamics of the wedge, only a few can be measured accurately. With a monitoring frequency of 10 Hz in the experiment, the coseismic phase, which spans roughly a tenth of a second in the simulation, is only covered by one or two measurements. We thus cannot hope to compare rates of slip, for example.

The following three quantities, in contrast, can be measured, and are properly resolved by the simulation.

3 Afterslip involves only relatively low velocities and has not been observed in the experiment due to limits in the resolution.

- Rupture width: The diameter of the region in which seismic velocities are reached (over the course of a single event).
- Peak slip: The maximum trenchward displacement at the base, which occurs at seismic velocities (over the course of a single event).
- Time of recurrence: The duration of time between the respective onsets of two consecutive events.

In their definition it is already assumed that we know what a seismic event is. The term shall mean here a contiguous time interval during which seismic velocities are attained at the base; a velocity, moreover, shall be called seismic if lies at least 1 mm/s above the plate convergence velocity.

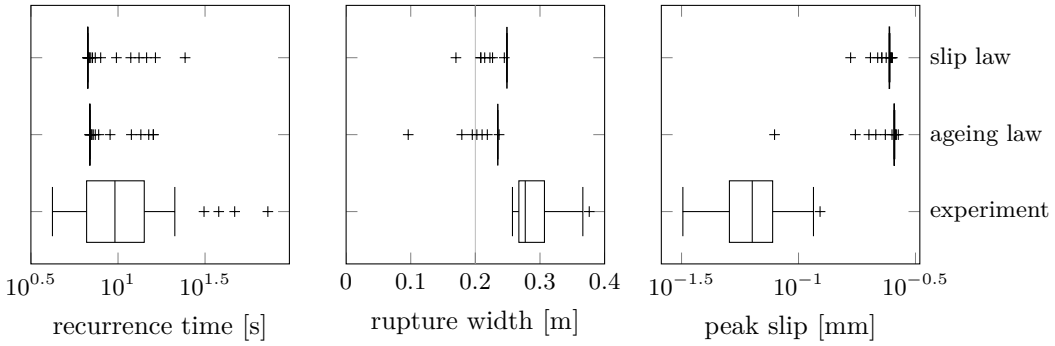

Figure 5.5: Some of the main quantities that describe earthquake rupture.

With these definitions in place, we can compare statistical data from experiment and simulation, based on 50 events which have been observed in the laboratory and approximately twice as many simulated events (102 with the ageing law, 106 with the slip law). Figure 5.5 shows the aforementioned quantities side-by-side, in box plot form.[4]

Apart from a few events that occur as the wedge passes through a transition period from stable loading to unstable sliding, there is no variability in the simulation — we see the same seismic cycle over and over again. The experimentally observed events, too, show little variation in frequency and magnitude, however.

Simulated and observed events have approximately the same frequence; their rupture widths differ by a slightly larger margin but the crucial feature of exceeding the seismogenic width and thus oversaturating the seismogenic zone is common to both settings. Peak slip differs considerably between simulation and experiment, unfortunately, but by less than an order of magnitude.

4 A dataset is represented by a (potentially rather thin) box with whiskers. The three vertical lines of any box each correspond to a quartile: the centre line indicates the median; the left (right) line indicates the point above (below) which 75 percent of the data can be found.

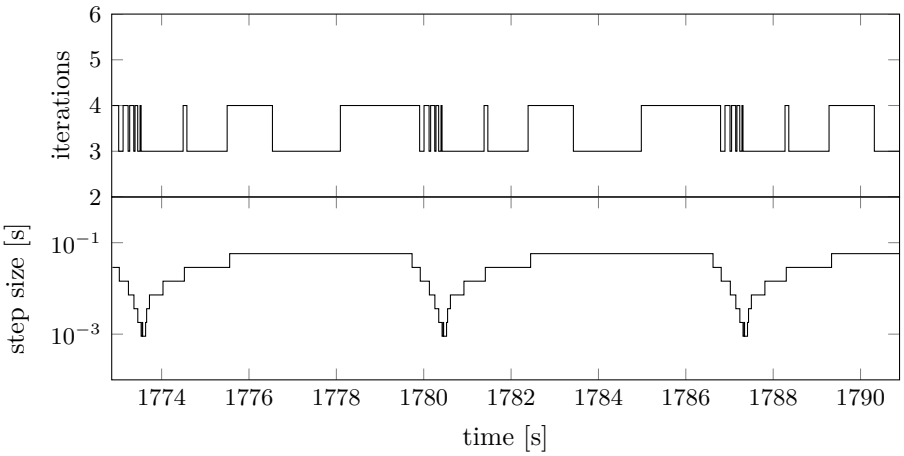

(a) Simulation based on the ageing law.

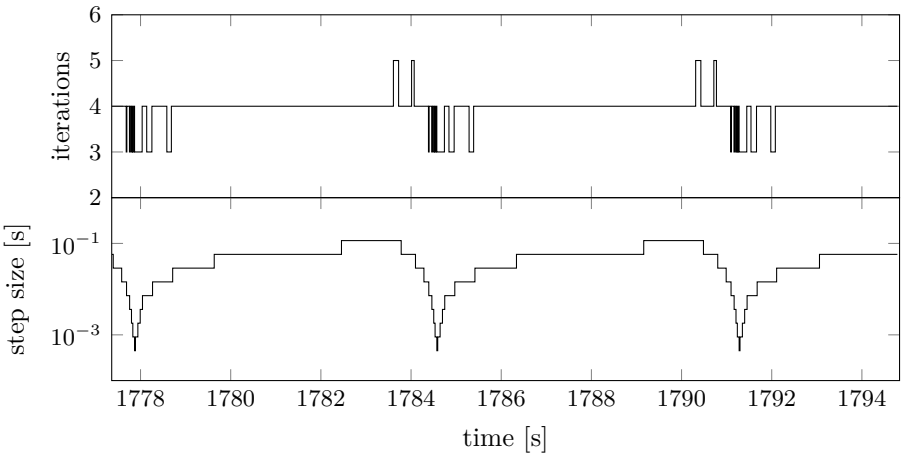

(b) Simulation based on the slip law.

Figure 5.6: Number of fixed point iterations in relation to the adaptive time step size over the course of a few seismic cycles.

Given the discrepancies in material properties and parameter uncertainties, better agreement cannot be expected.

5.5 STABILITY OF THE ALGORITHM

If the velocity field $\dot{\boldsymbol{u}}$ and the state field α vary rapidly in time, then they also exhibit a strong interdependence; in practice this means that for a given time step size, time-discrete problems with greater variation require a greater number of fixed point iterations.
This effect is compensated, however, by adaptive time stepping: In figure 5.6 we see how the number of fixed point iterations remains perfectly stable and almost constant in simulations with either the ageing law (2) or the slip law (3), through an appropriate resolution of the coseismic phase.

5.6 OUTLOOK

The preceding sections illustrate the capabilities of the framework and algorithm presented throughout this work.

Where to go from here?

We could aim for better agreement of simulation and experiment in order to validate one through the other. A different geometry that is more compatible with our mathematical framework would serve this purpose; an extension of the simulation to plastic materials would, too. It should also be mentioned that more complicated forms of rate-and-state friction than presented here have been proposed in which normal stress variations, as they can be expected to occur near the trench, are explicitly allowed and influence the state evolution.
First tests with three-dimensional domains or real-world scale parameters have been conducted and show promising results: The fixed point approach continues to work reliably also under these circumstances. The ability to handle such problems thus appears to hinge on the ability to solve large spatial problems quickly; work in this direction would, *e.g.*, enable us to study spatial rupture patterns as they emerge in subduction zones of greater thickness.
Finally, it would be desirable to learn more about rate-and-state friction in a time-continuous setting.

6 DISCUSSION OF ASSUMPTIONS

To turn a geophysical problem into a (tractable) mathematical problem, in the previous sections, I have made a few assumptions which are restrictive but indispensable. In addition, I have found it helpful to make a few more assumptions that are not strictly necessary or could be greatly weakened, but only at the cost of a more laborious and distracting notation.
In this chapter, therefore, each assumption is briefly discussed. In order of appearance, the following simplifications have been made:

- *The elasticity and viscosity tensors $\boldsymbol{\mathcal{B}}$ and $\boldsymbol{\mathcal{A}}$ are uniform.*[1] Guarantees that $\mathcal{K}$ and $\mathcal{C}$ are elliptic and bounded. Easily extended to tensors which vary in space, as long as their norm and ellipticity can be uniformly bounded.

- *Infinitesimal deformation.* While usually a very strong assumption which leads to a linear theory, it fits very well with problems of seismicity.

- *Bilateral contact.* Both μ and α depend on the *sliding velocity*, which necessitates permanent contact.

- *The normal stress σ_n is time-invariant (and thus known).* Already made in the derivation of the laws by Dieterich and Ruina. Reasonable, *e.g.*, if the body in question is covered by layers of heavy material.

- *The normal stress σ_n is uniform.* Can be allowed to vary in space, as long as it stays essentially bounded.

- *The friction parameters a, b, V_*, L, μ_* are uniform.* Purely for notational convenience. Easily extended to the case of functions on Γ_C which are uniformly bounded from above and away from zero.

- *The density ρ is uniform.* Guarantees that $\mathcal{M}$ is well-defined. The density could also vary in space, as long as multiplication with ρ maps $H^1(\Omega)$ into itself. In order to allow for less regular ρ, one needs to assume regularity of $\ddot{\boldsymbol{u}}$.

- *Homogeneous boundary conditions.* Purely for ease of presentation.

1 In what follows, a variable is called uniform if it does not vary in space.

A

NUMERICAL DETAILS

The numerical results from chapter 5 have been obtained from a computer code that is based on the DUNE framework, see also [2].

A.1 THE GRID

To construct a mesh on the domain Ω shown in figure 5.2 which resolves the seismogenic zone but not regions that can be assumed to have little effect on the sliding behaviour, starting from a single triangle, cells are repeatedly refined until they no longer exceed a prescribed maximum diameter m. For any cell, this diameter is given in terms of the distance d to the seismogenic region, the desired diameter m_{SZ} in the seismogenic zone itself, a characteristic length l, which is equal to the width of the wedge, and a growth factor s via

$$m = \left(\frac{d}{ls} + 1\right) \cdot m_{\mathrm{SZ}}.$$

The resolution of the resulting grid decreases linearly in the distance from the seismogenic zone. For $s = 8$ and $m_{\mathrm{SZ}} = 2\,\mathrm{mm}$, it contains 6563 vertices of which 262 lie on Γ_C; the smallest cells have a diameter of 1.01 mm, while the largest cell measures 64.74 mm across.

A.2 TOLERANCES

Apart from the grid resolution, three termination criteria control the accuracy of the numerical scheme:

- Problem 4.2 is considered accurately solved when two consecutive iterates are sufficiently close to one another in the sense of the energy norm induced by $\underline{\underline{\mathcal{Z}}}$.[1] The tolerance is chosen as $10^{-8}\,\mathrm{W}^{1/2}\mathrm{m}^{-1/2}$.
- The coupling in problem 4.3 is considered resolved when two consecutive state iterates differ only by $10^{-5}\,\mathrm{m}^{1/2}$ in the $L^2(\Gamma_C)$ norm.
- A time step is considered fine enough if its state field differs from the state field obtained with twice the resolution over the same period by no more than $10^{-5}\,\mathrm{m}^{1/2}$ in the $L^2(\Gamma_C)$ norm.

1 The term energy refers to the mathematical concept here, whose units generally do not correspond to physical energy.

A.3 ADAPTIVE TIME STEPPING

The third criterion is used to determine an appropriate time step adaptively as follows: Starting from the size of the previous time step, a time step of twice the size is considered. If this step is considered fine enough in the aforementioned sense, it is accepted, unless an even coarser time step can be found in the same manner, which is also feasible. If no coarsening can be carried out, the necessity to refine is considered, starting from a time step of half the original size.
The remaining details of the time stepping procedure correspond to the Newmark-β scheme (see table 3.1) with $\beta = 1/4$. The variable λ from (25) is chosen as 0.5.

B

MISCELLANEOUS THEOREMS

Proposition B.1. *Assume that the bounded domain $\Omega \subset \mathbb{R}^d$ has a Lipschitz boundary Γ, which is composed of two disjoint open subsets Γ_1 and Γ_2 as well as a connecting nullset. Then the space of functions*

$$\{\boldsymbol{v} \in H^{1/2}(\Gamma) \colon \boldsymbol{v} = 0 \text{ on } \Gamma_2\}$$

is dense in $L^2(\Gamma_1)$.

Proof. See Lemma 1.4 in [10]. □

Proposition B.2 (Korn)**.** *Assume that the bounded domain $\Omega \subset \mathbb{R}^d$ has a Lipschitz boundary. If $\mathcal{V}$ is a space that satisfies $H_0^1(\Omega)^d \subset \mathcal{V} \subset H^1(\Omega)^d$ and does not contain any nontrivial translations or rotations, then this implies*

$$\int_\Omega \|\boldsymbol{\varepsilon}(\boldsymbol{v})\|^2 \geq c \int_\Omega \|\nabla \boldsymbol{v}\|^2 \quad \text{for every } \boldsymbol{v} \in \mathcal{V}.$$

Proof. See Theorem 3.5 in [12]. □

Proposition B.3 (Rellich and Kondrachov)**.** *Assume that the bounded domain $\Omega \subset \mathbb{R}^d$ has a Lipschitz boundary Γ, which is composed of two disjoint open subsets Γ_1 and Γ_2 as well as a connecting nullset. Then we can define a trace operator*

$$\gamma_1 \colon H^1(\Omega)^d \to L^p(\Gamma_1)$$

for certain choices of $p \geq 1$: In two dimensions, any p is admissible, whereas in three dimensions, this is only possible for $p \leq 4$. Moreover, the operator

$$\gamma_1 \colon H^1(\Omega)^d \to L^s(\Gamma_1)$$

with extended codomain is compact whenever $s < p$.

Proof. See [3]. □

Proposition B.4 (Gronwall)**.** *Let $x \colon [0, \infty) \to \mathbb{R}$ be a differentiable function with $x(0) = 0$, whose derivative satisfies*

$$\dot{x} \leq a(t)x(t) + b \quad \text{for any } t \in [0, \infty),$$

where $a \leq 0$ is an integrable function and $b \geq 0$ is a constant. Then x satisfies

$$x(t) \leq x(0) + bt$$

for any $t \in [0, \infty)$.

Proof. Set $u(t) = x(t) - bt$, so that we only need to prove $u(t) \leq 0$, and note

$$\dot{u}(t) \leq ax(t) \leq ax(t) - abt = au(t). \tag{35}$$

The claim now follows from the differential form of Gronwall's lemma or simply from the observation that (35) implies $\dot{u} \leq 0$ whenever $u(t) = 0$. □

Proposition B.5 (Banach)**.** *Let X be a Banach space. If a map T on X is strictly contractive,* i.e. *q-Lipschitz with a constant $q < 1$, then it has a unique fixed point x_* and for any $x \in X$ we have*

$$T^n x \to x_* \quad \text{as } n \to \infty.$$

Proof. See Theorem 1.62 in [9]. □

Proposition B.6 (Schauder)**.** *Let K be a closed convex subset of a Banach space X. If $T\colon X \to X$ is continuous and maps K into itself, such that $T(K)$ is relatively compact in X, then T has a fixed point.*

Proof. See Corollary 11.2 in [5]. □

Proposition B.7. *Let $\mathcal{V}$ be a reflexive Banach space. If two convex, proper, lower semicontinuous functions F_1 and F_2 on $\mathcal{V}$ are given, and F_1 is additionally Gâteaux-differentiable, then the following conditions are equivalent.*

- *The vector $\boldsymbol{w}$ minimises $F_1 + F_2$ on $\mathcal{V}$.*
- *We have*
$$\langle F_1'(\boldsymbol{w}), \boldsymbol{v} - \boldsymbol{w}\rangle + F_2(\boldsymbol{v}) \geq F_2(\boldsymbol{w})$$
for every $\boldsymbol{w} \in \mathcal{V}$.

Proof. See Proposition 2.2 in Chapter II of [4]. □

Proposition B.8. *Let $\mathcal{V}$ be a real Hilbert space and consider the functional J given by*

$$J(\boldsymbol{v}) = \frac{1}{2} b(\boldsymbol{v}, \boldsymbol{v}) + j(\boldsymbol{v}) - \ell(\boldsymbol{v})$$

over $\mathcal{V}$, where b is a bounded $\mathcal{V}$-elliptic symmetric bilinear form, ℓ is a bounded linear functional, and j is a convex, proper, lower semicontinuous nonlinearity. This functional then has a unique minimiser.

Proof. See Corollary 4.6 in [9]. □

Proposition B.9. *Let $\boldsymbol{v}$ be an arbitrary H^1 function on a domain Ω. Then the function $\boldsymbol{v}^+$ given by*

$$\boldsymbol{v}^+(\boldsymbol{x}) = \max(0, \boldsymbol{v}(\boldsymbol{x})) \quad \text{for almost every } \boldsymbol{x} \in \Omega$$

lies in $H^1(\Omega)$ as well.

Proof. See Corollary 2.1.8 in [19]. A more general theorem about truncation of Sobolev functions can be found as Corollary 25.11 in [18]. □

Proposition B.10 (Levi)**.** *Let (Ω, μ, Σ) be a measure space. If a decreasing sequence of functions $\boldsymbol{v}_k \in L^1(\Omega, \mu)$ is given and $\boldsymbol{v} \coloneqq \inf_{k\in\mathbb{N}} \boldsymbol{v}_k$ lies in $L^1(\Omega, \mu)$, then $\boldsymbol{v}_n$ converges to $\boldsymbol{v}$ in $L^1(\Omega, \mu)$.*

Proof. See Theorem 11.1 in [17]. □

Proposition B.11 (Fatou)**.** *Let (Ω, μ, Σ) be a measure space. Then for any sequence of nonnegative functions $\boldsymbol{v}_k \in L^1(\Omega, \mu)$, which may take the value $+\infty$, we have*

$$\liminf_{j\to\infty} \int_\Omega \boldsymbol{v}_j \geq \int_\Omega \liminf_{j\to\infty} \boldsymbol{v}_j.$$

In other words, the integral operator is lower semicontinuous.

Proof. See Theorem 9.1 in [17]. □

Proposition B.12 (Krasnosel'skii)**.** *Let (Ω, μ, Σ) be a σ-finite measure space and $f\colon \mathbb{R}^d \times \Omega \to \mathbb{R}$ be such a map that $f(\boldsymbol{w}, \cdot\,)$ is measurable and $f(\cdot\,, \boldsymbol{x})$ is continuous for almost every $\boldsymbol{x} \in \Omega$ and $\boldsymbol{w} \in \mathbb{R}^d$. If we, furthermore, assume that the map*

$$\Omega \ni \boldsymbol{x} \mapsto f(\boldsymbol{w}(\boldsymbol{x}), \boldsymbol{x})$$

lies in $L^p(\Omega, \mu)$ for every $\boldsymbol{w} \in L^q(\Omega, \mu)$ with $1 \leq p, q < \infty$, then the $\boldsymbol{w}$-dependence of this map is continuous.

Proof. See Theorem 3.7 in [1]. □

C

GRADIENT FLOWS IN ONE DIMENSION

Consider an ordinary differential equation of the form

$$\dot{x} = f(x) \tag{36}$$

with a nonincreasing continuous function $f\colon \mathbb{R} \to \mathbb{R}$. We can then make the following observations.

- Equation (36) is uniquely solvable on the whole time interval $[0, \infty)$. Consequently, we can define a family of flow maps Φ_t that map initial data to the solution after a given time t.
- If f has exactly one zero x^*, then $\Phi_t x$ converges monotonically to x^* as $t \to \infty$, for any x.
- The function $t \mapsto |f(\Phi_t x)|$ is nonincreasing in t: If $f(\Phi_t x)$ is positive, then $\Phi_t x$ grows, so that $f(\Phi_t x)$ shrinks, and vice versa. Moreover, $f(\Phi_t x)$ can never change sign, since $\Phi_t x$ remains constant from any point s with $f(\Phi_s x) = 0$ on.
- Each flow-operator is nonexpansive, *i.e.*

  $$|\Phi_t x - \Phi_t y| \leq |x - y|$$

  holds for any x, y, and $t > 0$, since we have

  $$\frac{\mathrm{d}}{\mathrm{d}t}(\Phi_t x - \Phi_t y)^2 = 2(\Phi_t x - \Phi_t y)[f(\Phi_t x) - f(\Phi_t y)] \leq 0.$$

BIBLIOGRAPHY

[1] J. Appell and P. P. Zabrejko. *Nonlinear superposition operators*. Vol. 95. Cambridge Tracts in Mathematics. Cambridge: Cambridge University Press, 1990, pp. viii+311. ISBN: 0-521-36102-8. DOI: 10.1017/CBO9780511897450.

[2] P. Bastian et al. "A Generic Interface for Adaptive and Parallel Scientific Computing. Part II: Implementation and Tests in DUNE". In: *Computing* 82.2–3 (2 2008), pp. 121–138. ISSN: 0010-485X. DOI: 10.1007/s00607-008-0004-9.

[3] M. Biegert. "On traces of Sobolev functions on the boundary of extension domains". In: *Proceedings of the American Mathematical Society* 137.12 (2009), pp. 4169–4176. ISSN: 0002-9939. DOI: 10.1090/S0002-9939-09-10045-X.

[4] I. Ekeland and R. Temam. *Convex analysis and variational problems*. Amsterdam: North-Holland Publishing Co., 1976, pp. ix+402.

[5] D. Gilbarg and N. S. Trudinger. *Elliptic partial differential equations of second order*. Vol. 224. Grundlehren der Mathematischen Wissenschaften. Berlin: Springer-Verlag, 1977, pp. x+401. ISBN: 3-540-08007-4.

[6] C. Gräser, U. Sack, and O. Sander. "Truncated Nonsmooth Newton Multigrid Methods for Convex Minimization Problems". In: *Domain Decomposition Methods in Science and Engineering XVIII*. Ed. by M. Bercovier et al. Vol. 70. Lecture Notes in Computational Science and Engineering. Selected papers from the 18th International Conference held at the Hebrew University of Jerusalem, Jerusalem, January 12–17, 2008. Springer-Verlag, Berlin, 2009, pp. 129–136. ISBN: 978-3-642-02677-5. DOI: 10.1007/978-3-642-02677-5_12.

[7] C. Gräser and O. Sander. "TNNMG methods for block-separable minimization problems". In preparation.

[8] W. Han and B. D. Reddy. *Plasticity*. 2nd ed. Vol. 9. Interdisciplinary Applied Mathematics. Mathematical theory and numerical analysis. New York: Springer, 2013, pp. xvi+421. ISBN: 978-1-4614-5939-2; 978-1-4614-5940-8. DOI: 10.1007/978-1-4614-5940-8.

[9] W. Han and M. Sofonea. *Quasistatic contact problems in viscoelasticity and viscoplasticity*. Vol. 30. AMS/IP Studies in Advanced Mathematics. Providence, RI: American Mathematical Society, 2002, pp. xviii+442. ISBN: 0-8218-3192-5.

[10] R. Hünlich and J. Naumann. “On general boundary value problems and duality in linear elasticity. I”. In: *Aplikace Matematiky* 23.3 (1978), pp. 208–230. ISSN: 0373-6725.

[11] Ch. Marone. “Laboratory-derived friction laws and their application to seismic faulting”. In: *Annual Review of Earth and Planetary Sciences* 26.1 (1998), pp. 643–696. DOI: 10.1146/annurev.earth.26.1.643.

[12] J. Nečas and I. Hlaváček. *Mathematical theory of elastic and elasto-plastic bodies: an introduction*. Vol. 3. Studies in Applied Mechanics. Amsterdam: Elsevier Scientific Publishing Co., 1980, p. 342. ISBN: 0-444-99754-7.

[13] E. Pipping, O. Sander, and R. Kornhuber. “Variational formulation of rate- and state-dependent friction problems”. In: *Zeitschrift für Angewandte Mathematik und Mechanik* (2013). ISSN: 1521-4001. DOI: 10.1002/zamm.201300062.

[14] J. R. Rice, N. Lapusta, and K. Ranjith. “Rate and state dependent friction and the stability of sliding between elastically deformable solids”. In: *Journal of the Mechanics and Physics of Solids* 49.9 (2001), pp. 1865–1898. ISSN: 0022-5096. DOI: 10.1016/S0022-5096(01)00042-4.

[15] M. Rosenau, J. Lohrmann, and O. Oncken. “Shocks in a box: An analogue model of subduction earthquake cycles with application to seismotectonic forearc evolution”. In: *Journal of Geophysical Research: Solid Earth* 114.B1 (2009). ISSN: 2156-2202. DOI: 10.1029/2008JB005665.

[16] M. Rosenau et al. “Experimental insights into the scaling and variability of local tsunamis triggered by giant subduction megathrust earthquakes”. In: *Journal of Geophysical Research: Solid Earth* 115.B9 (2010). ISSN: 2156-2202. DOI: 10.1029/2009JB007100.

[17] R. L. Schilling. *Measures, integrals and martingales*. Cambridge University Press, New York, 2005, pp. xii+381. ISBN: 978-0-521-61525-9; 0-521-61525-9. DOI: 10.1017/CBO9780511810886.

[18] H. Triebel. *The structure of functions*. Vol. 97. Monographs in Mathematics. Birkhäuser Verlag, Basel, 2001, pp. xii+425. ISBN: 3-7643-6546-3. DOI: 10.1007/978-3-0348-8257-6.

[19] W. P. Ziemer. *Weakly differentiable functions*. Vol. 120. Graduate Texts in Mathematics. Sobolev spaces and functions of bounded variation. Springer-Verlag, New York, 1989, pp. xvi+308. ISBN: 0-387-97017-7. DOI: 10.1007/978-1-4612-1015-3.

ZUSAMMENFASSUNG

In der vorliegenden Arbeit wird das Modell geschwindigkeits- und zustandsabhänger Reibung, welches von zentraler Bedeutung für numerische Erbebensimulationen ist, von einem mathematischen Gesichtspunkt untersucht.

Zunächst werden bekannte Gesetze in eine abstrakte Struktur eingeordnet, auf Grundlage derer sie oder vergleichbare Reibungsgesetze verstanden und analysiert werden können. Innerhalb dieses Rahmens wird dann ein viskoelastisches Problem formuliert, sowohl in starker als auch in schwacher Form, das sich aus der Modellierung erdbebentypischen Rutschens entlang einer Störungszone ergibt.
Eine Analyse gestaltet sich, aufgrund der Variablenkopplung, die das untersuchte Reibungsmodell mit sich bringt, schwierig. Im Zeitdiskreten lassen sich jedoch sowohl Aussagen über Existenz und Eindeutigigkeit von Lösungen als auch über stetige Parameterabhängigkeit tätigen.
Die zugrundeliegende Idee dabei ist es, eine Variablenkopplung als Fixpunktproblem aufzufassen und die Konvergenz einer zugehörigen Iteration zu zeigen. Darauf basierend wird ein Algorithmus vorgeschlagen, der das Problem mithilfe einer Fixpunktiteration entkoppelt. Durch den Einsatz eines modernen Lösers und adaptiver Zeitschrittsteuerung ergibt sich so ein Verfahren, das nicht nur stabil sondern auch schnell ist.
Seine Anwendbarkeit auf relevante Probleme wird im Folgekapitel unter Beweis gestellt, das sich auf die Simulation von Megathrust-Erdbeben konzentriert, wie sie an der Sohle einer Subduktionszone auftreten.

Das letzte Kapitel schließlich fasst die Annahmen zusammen, die in den vorgehenden Kapitel getroffen werden.

EIDESSTATTLICHE ERKLÄRUNG

Für die Verfassung der vorliegenden Arbeit wurden keine anderen als die im Text aufgeführten Hilfsmittel verwendet.
Diese Arbeit ist des Weiteren zu keinem früheren Zeitpunkt in einem Promotionsverfahren eingereicht worden.

Berlin, September 2014

Elias Pipping